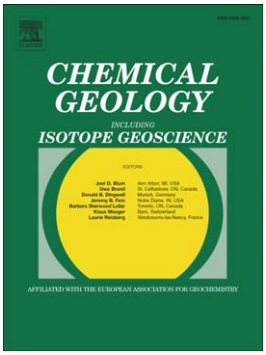

Structural limitations in deriving accurate U-series ages from calcitic cold-water corals contrasts with robust coral radiocarbon and Mg/Ca systematics

Marcus Gutjahr, Derek Vance, Dirk L. Hoffmann, Claus-Dieter Hillenbrand, Gavin L. Foster, James W.B. Rae, Gerhard Kuhn

PII: S0009-2541(13)00294-5
DOI: doi: 10.1016/j.chemgeo.2013.07.002
Reference: CHEMGE 16938

To appear in: *Chemical Geology*

Received date: 15 November 2012
Revised date: 1 July 2013
Accepted date: 4 July 2013

Please cite this article as: Gutjahr, Marcus, Vance, Derek, Hoffmann, Dirk L., Hillenbrand, Claus-Dieter, Foster, Gavin L., Rae, James W.B., Kuhn, Gerhard, Structural limitations in deriving accurate U-series ages from calcitic cold-water corals contrasts with robust coral radiocarbon and Mg/Ca systematics, *Chemical Geology* (2013), doi: 10.1016/j.chemgeo.2013.07.002

Structural limitations in deriving accurate U-series ages from calcitic cold-water corals contrasts with robust coral radiocarbon and Mg/Ca systematics

Marcus Gutjahr[1, 2*], Derek Vance[1,3], Dirk L. Hoffmann[4, 5], Claus-Dieter Hillenbrand[6], Gavin L. Foster[7], James W.B. Rae[1]and Gerhard Kuhn[8]

[1] Bristol Isotope Group, Dep. of Earth Sciences, University of Bristol, Queens Rd, Bristol BS8 1RJ, UK

[2] now at: GEOMAR Helmholtz Centre for Ocean Research Kiel, Wischhofstrasse 1-3, 24148 Kiel, Germany

[3] now at: ETH Zürich, Institute of Geochemistry and Petrology, Department of Earth Sciences, NW D81.4, Clausiusstrasse 25, 8092 Zürich, Switzerland

[4] Bristol Isotope Group, School of Geographical Sciences, University of Bristol, University Rd, Bristol, BS8 1SS, UK

[5] CENIEH, Paseo Sierra de Atapuerca s/n, 09002 Burgos, Spain

[6] British Antarctic Survey, High Cross, Madingley Road, Cambridge CB3 0ET, UK

[7] Ocean and Earth Science, University of Southampton, European Way, Southampton, SO14 3ZH, UK

[8] Alfred Wegener Institute for Polar and Marine Research, Am Alten Hafen 26, 27568 Bremerhaven, Germany

[*] *Corresponding author: mgutjahr@geomar.de*

Abstract

Radiocarbon and uranium-thorium dating results are presented from a genus of calcitic Antarctic cold-water octocorals (family *Coralliidae)*, which were collected from the Marie Byrd Seamounts in the Amundsen Sea (Pacific sector of the Southern Ocean) and which to date have not been investigated geochemically. The geochronological results are set in context with solution and laser ablation-based element/Ca ratios (Li, B, Mg, Mn, Sr, Ba, U, Th).

Octocoral radiocarbon ages on living corals are in excellent agreement with modern ambient deep-water $\Delta^{14}C$, while multiple samples of individual fossil coral specimens yielded reproducible radiocarbon ages. Provided that local radiocarbon reservoir ages can be derived for a given time, fossil Amundsen Sea octocorals should be reliably dateable by means of radiocarbon.

In contrast to the encouraging radiocarbon findings, the uranium-series data are more difficult to interpret. The uranium concentration of these calcitic octocorals is an order of magnitude lower than in the aragonitic hexacorals that are conventionally used for geochronological investigations. While modern and Late Holocene octocorals yield initial $\delta^{234}U$ in good agreement with modern seawater, our results reveal preferential inward diffusion of dissolved alpha-recoiled ^{234}U and its impact on fossil coral $\delta^{234}U$. Besides alpha-recoil related ^{234}U diffusion, high-resolution sampling of two fossil octocorals further demonstrates that diagenetic uranium mobility has offset apparent coral U-series ages. Combined with the preferential alpha-recoil ^{234}U diffusion, this process has prevented fossil octocorals from preserving a closed system U-series calendar age for longer than a few thousand years. Moreover, several corals investigated contain significant initial thorium, which cannot be

adequately corrected for because of an apparently variable initial $^{232}Th/^{230}Th$. Our results demonstrate that calcitic cold-water corals are unsuitable for reliable U-series dating.

Mg/Ca ratios within single octocoral specimens are internally strikingly homogenous, and appear promising in terms of their response to ambient temperature. Magnesium/lithium ratios are significantly higher than usually observed in other deep marine calcifiers and for many of our studied corals are remarkably close to seawater compositions.

Although this family of octocorals is unsuitable for glacial deep-water $\Delta^{14}C$ reconstructions, our findings highlight some important differences between hexacoral (aragonitic) and octocoral (calcitic) biomineralisation. Calcitic octocorals could still be useful for trace element and some isotopic studies, such as reconstruction of ambient deep water neodymium isotope composition or pH, via boron isotopic measurements.

Keywords: Radiocarbon, U-series dating, cold-water corals, Southern Ocean, radiocarbon ventilation age, octocoral, Mg/Ca, Mg/Li, vital effect, high-Mg calcite, uranium diffusion

1. Introduction

Pleistocene glacial-interglacial fluctuations in atmospheric carbon dioxide (pCO_2) concentrations are tightly connected to variations in global overturning circulation and resulting variable ocean-atmosphere net CO_2 exchange fluxes (Archer et al., 2000; Brovkin et al., 2007; Anderson et al., 2009). The detection of temporal changes in Dissolved Inorganic Carbon (DIC) concentrations in intermediate and deep water is key in this context, and can, in theory, be tracked by analysing carbon cycle-dependent proxies, such as boron ($\delta^{11}B$) or carbon ($\delta^{13}C$) isotopic compositions, as well as relative past deep water radiocarbon

concentrations ($\Delta^{14}C$) in biogenic carbonate. Deep and intermediate ocean $\Delta^{14}C$ records are particularly useful for resolving the effect of deep ocean carbon storage (Adkins et al., 1998; Mangini et al., 1998; Sikes et al., 2000; Goldstein et al., 2001; Robinson et al., 2005; Marchitto et al., 2007; Skinner et al., 2010; Burke and Robinson, 2012). Many of these studies used scleractinian cold water corals as palaeoceanographic archives. Yet collection of scleractinian corals is difficult, often serendipitous, and expensive, and as a result large parts of the world's ocean remain unsampled. Given the scarcity of suitable sampling sites in key oceanographic areas, other coral species need to be tested in order to gain better access to, and geographical coverage of, glacial-interglacial deep sea chemistry and carbon cycle parameters.

For any study using fossil cold-water corals the determination of accurate calendar ages (i.e. coral calcification ages) independent of ^{14}C dating is a prerequisite for reconstructing changes in the deep ocean radiocarbon budget. Uranium-thorium (U-Th) disequilibrium ages of scleractinian cold-water corals provide such chronologies because of the long residence time of dissolved uranium in seawater (200-400 ka) and the isotopic enrichment of ^{234}U relative to ^{238}U, resulting in a homogenous modern seawater $\delta^{234}U$ of ~146.8 ± 0.1 ‰ (Andersen et al., 2010). This ambient seawater $^{234}U/^{238}U$ isotopic composition is incorporated into the coral carbonate and, if behaving as a closed system, the coral $^{234}U/^{238}U$ and $^{230}Th/^{238}U$ provide robust age information (Edwards et al., 1987). However, many fossil corals display open system behaviour, suggesting that the U isotopic composition has been modified after growth (Henderson, 2002; Pons-Branchu et al., 2005; Robinson et al., 2005; Scholz and Mangini, 2007). On the other hand, numerous other fossil scleractinian corals *do* display closed-system behaviour, and thus provide highly relevant palaeoceanographic and palaeoclimatic archives.

Geochemical and isotopic Amundsen Sea scleraxonian cold-water coral study

The aim of this paper is to evaluate the reliability of a family of calcitic cold-water octocorals, whose specimens were collected from the Marie Byrd Seamounts in the Amundsen Sea (West Antarctica), for deep-sea $\Delta^{14}C$ reconstructions by means of coupled U-Th disequilibria and radiocarbon age measurements. Furthermore, an elemental characterisation of these corals is provided to assess differences in biomineralisation compared with scleractinian cold-water corals (e.g., Adkins et al., 1998; Robinson et al., 2005; Mangini et al., 2010). Although a comprehensive calibration cannot be provided with the coral samples investigated in this study, Mg/Ca and Mg/Li from modern and fossil coral specimens are also presented in order to assess the potential of this genus for deep-ocean temperature reconstructions (cf. Case et al., 2010; Raddatz et al., in press). The specimens investigated here are expected to have recorded the water mass properties of Circumpolar Deep Water (CDW) during growth.

2. Area Description, Methods and Material

The calcitic cold-water scleraxonian octocorals used in this study were sampled south of the Antarctic Polar Front and are derived from the Marie Byrd Seamounts in the Amundsen Sea in the Pacific sector of the Southern Ocean (~123ºW, ~69ºS, 2500 m to 1430 m water depth) (Fig. 1; Table 1). These calcitic cold-water octocorals belong to the family *Coralliidae*. Corals were dredged during scientific cruises of RV *Polarstern* in 2006 (ANT-XXIII/4) (Gohl, 2006) and 2010 (ANT-XXVI/3) (Gohl, 2010).

Individual coral specimens were cut at the University of Bristol using a band saw for coarse sampling and a wire saw for fine sampling, and subsequently polished using grinding paper of various grain sizes. All samples were ultrasonicated in deionised water (18.2 MΩ) for 10 minutes to remove surface contaminants from the grinding process. Polished cross-sections

were prepared for laser ablation analysis. In order to avoid internal growth hiatuses, only visually pristine interior sections were chosen for U-Th- and radiocarbon dating (see Fig. 2) as well as additional solution-based elemental concentration ratio measurements. One half of a coral sample was used for U-Th isotopic analyses and the other half for laser ablation studies.

2.1 Radiocarbon AMS dating

Reductively pre-cleaned coral sub-samples prepared at Bristol University were sent to the Laboratory of Ion Beam Physics at the Federal Institute of Technology Zürich (ETHZ) for radiocarbon AMS dating. A short leaching (10 min) in 3% H_2O_2 was applied and samples were afterwards washed and dissolved in concentrated H_3PO_4. Further analytical details can be found in Hajdas et al. (2004a; 2004b) and Nemec et al. (2010). Details of AMS mass spectrometry can be found in Wacker et al. (2010). Individual coral radiocarbon results are displayed in Table 2. Conventional radiocarbon ages were obtained by subtracting the modern radiocarbon reservoir effect determined on living coral specimens and converted into calibrated calendar ages following Fairbanks et al. (2005).

2.2 U-series methods

Coral sub-samples ranging in size from 50 to 500 mg were used for U-Th isotopic analyses. Although Fe-Mn oxyhydroxides were not detectable during visual inspection, cut samples were reductively cleaned using a 0.01M ascorbic-acid – 0.062 Na_2EDTA mixture in acid-cleaned 1.5 ml centrifuge vials in a water bath at 70°C for 60 minutes (Lomitschka and Mangini, 1999). During this procedure samples were ultrasonicated for 20 seconds every 10 minutes. Subsequently samples were rinsed twice with 18.2 MΩ MQ water and dried in a clean room environment. After weighing, samples were transferred into 15 ml teflon vials

and 1-2 ml distilled water and a mixed $^{229}Th/^{236}U$ in-house spike were added. Coral samples were then carefully dissolved by dropwise addition of concentrated HNO_3. Samples were dried once more after dissolution, and carbonate-hosted organics oxidised by refluxing samples in a 1:1 mixture of suprapure concentrated HNO_3 and 30% H_2O_2 for at least 24 hours at 160°C in closed vials. Solutions were not viscous after the refluxing treatment, confirming that most/all organic material had been oxidised.

Purification of Th and U fractions was carried out using a two-column procedure. First, dried samples were dissolved in dilute (1.5M) HNO_3 and the U plus Th fraction separated from the carbonate matrix and most other trace constituents using Eichrom TRU resin following Luo et al. (1997). Thorium and U were then separated from each other on a second column separation step using AG1-X8 anion exchange resin (Chen et al., 1986). Both U and Th fractions were refluxed once more in a 1:1 mixture of suprapure concentrated HNO_3 and 30% H_2O_2 for at least 24 hours at 160°C in closed vials to destroy potential residual organics derived from the ion exchange resin prior to mass spectrometric analyses.

All Th and U isotope analyses were carried out on a Thermo-Finnigan Neptune MC-ICPMS at the Bristol Isotope Group (BIG) laboratory following the routine of Hoffmann et al. (2007). Uranium and Th isotopes were determined using a standard-sample-bracketing routine in separate measurements. Uranium standard solution NBL-112a was used for the mass-bias and ion counter gain corrections during U isotopic analyses, whereas an in-house ^{229}Th-^{230}Th-^{232}Th "TEDDi" Th standard solution was employed to bracket Th isotopic analyses (TEDDi: $^{230}Th/^{229}Th=1.519\pm0.002$, $^{230}Th/^{232}Th=(4.444\pm0.007) \times 10^{-3}$, $^{229}Th/^{232}Th=(2.927\pm0.005) \times 10^{-3}$; all ratios are atomic (Hoffmann et al., 2007)). Major isotopes (^{235}U, ^{238}U) were measured on Faraday collectors, whereas minor isotopes (^{229}Th,

^{230}Th, ^{234}U, ^{236}U) were measured on a Secondary Electron Multiplier (SEM) located behind an energy and angular filtering device (Retarding Potential Quadrupole – RPQ). Due to low concentrations in most samples, coral-hosted ^{232}Th was also measured on the SEM, whereas the bracketing TEDDi standard ^{232}Th was determined on a Faraday collector. Ion counter dead noise, peak tailing from ^{238}U, hydride-and oxide formation were monitored on a session-by-session basis. Sample gas settings were tuned for maximum stability instead of maximum sensitivity. In order to assure best washout behaviour, samples and standards were run in 0.6M HCl, with an additional 0.6M HCl – 0.05M HF wash step preceding a 0.6M HCl washout routine between samples/standards. Uranium-Thorium isotopic results are displayed in Table 3. Coral U-Th isotope compositions were converted into ages using the program 'isoplot' version 3.0 (Ludwig, 2003). Initial water column derived ^{230}Th was corrected for using the measured [^{232}Th] and a local Amundsen Sea water column estimate of the atomic ^{232}Th/^{230}Th of 5,000, obtained from earlier cold-water coral work from the Drake Passage (Goldstein et al., 2001; Burke and Robinson, 2012). For two of the fossil coral specimens, use of this initial ^{232}Th/^{230}Th led to an over-correction. Hence due to the lack of better Th isotopic constraints an arbitrary atomic ^{232}Th/^{230}Th ratio of 10,000 was used instead (marked in Table 3). Besides, in order to resolve the effects of variable initial ^{232}Th/^{230}Th$_{(0)}$, the correction using typical CDW ^{232}Th/^{230}Th estimates was only carried out for fossil corals and not for modern specimens, since we were also interested in monitoring modern water column ^{232}Th/^{230}Th inheritance and variability. As discussed in section 4.2 below, modern corals had initial ^{232}Th/^{230}Th closer to typical crustal compositions than most of the fossil corals.

A fine-scale ^{234}U/^{238}U isotopic analysis was carried out on coral specimen *PS69/318-1-4*. For this purpose, less than one milligram of coral material was drilled per sample using a NewWave Research MicroMill in the Department of Archaeology and Anthropology at the

University of Bristol. Unspiked purified samples were mass-bias and ion counter gain-corrected using NBL-112a as a bracketing standard. The external reproducibility of these measurements at ion currents on the order of 0.05 to 0.12 x 10^{-11} A for ^{238}U as well as ^{234}U ion currents ranging from 180 to 380 cps on the SEM were assessed by concentration-matched standard runs of an in-house secondary U-standard and found to be precise to an $(^{234}U/^{238}U)_{ACT}$ of 0.012 (2σ, n=4).

2.3 Solution-based and laser ablation elemental mapping

A small fraction of several corals analysed for their U-series isotope systematics have also been analysed for their major and trace elemental ratios (e.g., Li, Mg, Ca, Sr, Ba) (Table 4) on a ThermoFinnigan Element2 ICP-MS. The following isotopes were measured: ^{7}Li, ^{25}Mg, ^{43}Ca, ^{88}Sr and ^{138}Ba in low-resolution mode. Sample concentrations were normalised to bracketing in-house matrix-matched standard concentrations run at standard/sample Ca concentration on the order of 1 mmol/l. The external reproducibilities of these element-to-calcium ratios are typically better than 5% at 2 SD.

Laser ablation analyses were conducted at BIG using a New Wave Research UP193HE ArF Excimer laser system connected to the same Thermo-Finnigan Element2. Coral specimens analysed by means of laser ablation techniques were placed in epoxy, polished using P1200 abrasive grinding paper, scanned and placed in a laser ablation cell flushed with helium carrier gas (~1 L/min). Sample compositions were measured relative to NIST610 standard material that was used as the normalising standard. Additionally, a secondary NIST612 standard was measured for comparison. Analyses were run in automated sequences in two blocks of 20 samples using ^{43}Ca as internal standard for both samples and standards, always bracketed by two NIST610 and NIST612 standard measurements before and after the sample

runs. The laser system has a wavelength of 193 nm and a typical power density on the order of 5 J/cm^2 at 70% power output. Coral sample laser ablation acquisition settings were chosen as 130 μm spots, 5 Hz, 60% power output lasering for 60 seconds, 30 seconds blank measurements, 60 seconds washout. The laser ablation measurements of the bracketing NIST standard ablation settings differed only in their spot size (70 μm as opposed to 130 μm), the remaining settings being kept identical to the sample runs. The first few seconds of the ablation pass were excluded for each sample/standard using the time-resolving Glitter laser ablation data reduction software (http://www.glitter-gemoc.com). Results obtained for SRM NIST612 elemental ratios are displayed in Table 5 alongside their deviation from GeoRem preferred values (Jochum et al., 2011).

3. Results

3.1 Radiocarbon dates

The modern Amundsen Sea radiocarbon reservoir effect (i.e., R+ΔR) in intermediate water depth at the Marie Byrd Seamounts, as recorded by cold-water corals, was assessed through analysis of two modern specimens that were alive at the time of dredging. An entire chemically cleaned cross-section of the main stem of *PS69/319-1-modern* as well as the internal part (ca. 2 mm from the outer rim) of *PS75/247-2-modern* (see Fig. 2) was sampled and the radiocarbon results are shown in Table 2. The first sample was dredged from a water depth between 2009 m and 1475 m, whereas the second sample was recovered from a water depth between 1708 m and 1504 m.

The average conventional radiocarbon age of sample *PS69/319-1-modern* is younger than that of *PS75/247-2-modern* by 118 conventional ^{14}C years (mean value of 1391 yr ^{14}C as opposed to 1509 yr ^{14}C). The average radiocarbon reservoir age of *PS69/319-1-modern* is in

excellent agreement with both previous estimates of the modern reservoir effect in CDW (e.g. Berkman and Forman, 1996) and direct seawater radiocarbon data. The local ambient water radiocarbon concentration at 69°S, 120° W is reported as $\Delta^{14}C$ of -158 ‰ in 1500 m water depth and -163 ‰ in 2000 m in the GLODAP database (http://cdiac3.ornl.gov). This value corresponds to a local modern radiocarbon reservoir effect of 1381 years in 1500 m and 1429 years in 2000 m water depth. The slightly older ^{14}C age in the interior of sample *PS75/247-2-modern* might result from slow growth rates of the corals, i.e. this sample may comprise a sub-recent inner section within a coral that was alive during dredging.

To date, growth rates for the genus presented here have not been published. Roark et al. (2009) reported extremely slow growth rates for proteinacous octocorals *Gerardia sp.* (36 ± 20 μm/yr) and *Leiopathes sp.* (<5 μm/yr) in circa 300-500 m water depth offshore Hawaii. Cold-water coral growth rates will also depend on seawater temperature (e.g., Matsumoto, 2007). The ambient potential temperature along the Marie Byrd Seamounts in 1500 m water depth as measured at CTD station *PS75/253-1* on cruise ANT-XXVI/3 in March 2010 is 0.91°C possibly resulting in slow growth rates. Besides, in contrast to scleractinian deep-water corals, the internal calcitic skeleton of the octocorals from the Marie Byrd Seamounts is very dense (Fig. 2), which is probably a side effect of slow growth.

The ^{14}C ages of fossil corals presented in Table 2 suggest three distinct growth periods: (i) from 14.21 cal ka BP to present, (ii) from ~40 to ~37 cal ka BP, and (iii) from ~49 to ~45 cal ka BP (Fig. 3). The radiocarbon reservoir effect at intermediate water depths in the Southern Ocean probably varied over the past 50 ka because of large-scale glacial-interglacial changes in strength, latitudinal position and upwelling vigour within the Antarctic Circumpolar Current (e.g., Toggweiler et al., 2006; Anderson et al., 2009; Skinner et al., 2010). Therefore

only approximate ages are provided here, and error bars on Fig. 3 reflect the maximal uncertainties on the radiocarbon reservoir effect. Calibrated calendar ages shown in Table 2 were calculated using (a) a modern radiocarbon reservoir effect (1391 yr ^{14}C, corresponding to the mean ^{14}C age of *PS69/319-1-modern*), (b) a likely realistic late glacial as well as early deglacial radiocarbon reservoir effect of 2000 yr and (c) a more extreme value of 2500 yr. Reservoir ages similar to the present-day are justified for at least the last 6 ka (Hall et al., 2010), and were likely extant since the Antarctic Cold Reversal (ACR, ca. 14.7 to 12.76 ka BP; Stenni et al., 2011) (see discussion below), while the early deglacial and glacial reservoir age may be on the order of 2 kyr ^{14}C or more (Burke and Robinson, 2012).

Three fossil coral specimens sampled multiple times at high (mm-scale) spatial resolution also provide very consistent ^{14}C ages. Coral *PS69/318-1-4* has been sampled ten times in two separate sections that were cut from the original coral circa 8 cm apart (Table 2). The average conventional ^{14}C age of all samples is 12,055 +/- 221 yr (2 s.d., n=10). Both sections show a tendency towards younger ages in the outer parts of the coral. Growth rates on the order of only a few μm/yr are therefore consistent with the ^{14}C age range of specimen *PS69/318-1-4*.

3.2 Uranium-series characteristics

A total of 51 individual U-series analyses were carried out, aiming to provide U and Th concentrations as well as U-Th disequilibrium dates. An overview of the coral U-series data is presented in Table 3 and Figure 4a. For most individual specimens one or two sub-samples were prepared. Two coral specimens were analysed at higher spatial resolution (n=16; n=10) (Figs. 4c and d, 5, 6). Two modern corals shown in Fig. 2 were also analysed in order to assess the octocoral carbonate ^{234}U/^{238}U in comparison with present-day seawater and to determine the incorporation of water column derived initial ^{230}Th and ^{232}Th during growth.

The U concentrations in the studied octocorals are typically an order of magnitude lower than in their scleractinian aragonitic counterparts (e.g., Goldstein et al., 2001; Robinson et al., 2005), ranging from 25 ng/g to 268 ng/g (Table 3). Isotopically, modern coral $(^{234}U/^{238}U)_{ACT}$ agree within error with present-day seawater composition ($(^{234}U/^{238}U)_{SW} = 1.1468 \pm 0.0001$) (Andersen et al., 2010) confirming isotopically-congruent incorporation of seawater-derived U into the coral carbonate matrix. The two modern specimens contain sub-ppb concentrations of ^{232}Th (0.05 to 0.51 ng/g) and low [^{230}Th] ($0.0028 \leq (^{230}Th/^{238}U)_{ACT} \leq 0.0062$). Non-zero modern mean U-series ages were recorded for *PS69/319-1-modern* (260 ± 30, while the mean age of *PS75/247-2-modern* is 170 ± 270 a (Fig. 4b, Table 3).

For the modern corals the water column-derived Th contributions (i.e., initial Th) were determined. Calculating the initial coral $^{232}Th/^{230}Th$ according to Cheng et al. (2000) (their Eq. 4) results in initial atomic $^{232}Th/^{230}Th_{(0)}$ of 26,500 and 81,600 for *PS69/319-1-modern* and $^{232}Th/^{230}Th_{(0)}$ of 55,300 and 233,700 for *PS75/247-2-modern*. These initial Th isotopic compositions are quite variable and significantly higher than $^{232}Th/^{230}Th_{(0)}$ ratios reported for cold-water corals from the Drake Passage ($^{232}Th/^{230}Th_{(0)}$ ~5,000; Goldstein et al., 2001; Burke and Robinson, 2012). Apart from two exceptions, these elevated $^{232}Th/^{230}Th_{(0)}$ do not appear to be representative of initial Th as measured in most fossil Amundsen Sea cold-water corals (see Table 3 and discussion in section 4.2).

Most of the corals yielding U-series ages younger than 5 ka have $(^{234}U/^{238}U)_{initial}$ within error of, or close to (within less than 7 ‰), modern seawater compositions (Table 3). One fossil coral specimen (*PS69/312-1-1*) had elevated present-day and initial $(^{234}U/^{238}U)_{ACT}$ yet reproducible apparent U-series ages (mean: 4.14 ± 0.2 ka; n=2). Virtually all remaining coral

samples presented in Table 3 fail this closed-system screening test (Stirling and Andersen, 2009). Two broad trends can be identified: (i) fossil corals have elevated ($^{234}U/^{238}U$) as well as (ii) sometimes highly enriched ($^{230}Th/^{238}U$), usually accompanied by similar enrichments in ^{232}Th (Table 3, Figs. 4, 7). Despite significant variability between the individual specimens, in most cases the [^{238}U] in fossil corals is higher than in their modern counterparts. The two modern specimens have average [^{238}U] of ~40 ng/g, while the average [^{238}U] in fossil corals is 94 ± 65 ng/g (2 s.d., n=16, average [^{238}U] used for every fossil coral specimen). The majority of the apparent U-series ages presented in Table 3 are regarded as unreliable (see discussion in section 4.2).

3.3 Coral-hosted Mg/Ca and Mg/Li

Solution-based coral Mg/Ca ratios for samples shown in Table 4 range from 70.7 mmol/mol to 82.6 mmol/mol, while the laser ablation scan shown in Figure 8 carried out on the Holocene section (outer part) of *PS69/321-1-2* suggests a Mg/Ca ratio around 100 mmol/mol (solution-based composition of the Holocene segment of this coral: 82.6 mmol/mol). The lowest overall Mg/Ca ratio, observed in an overgrown coral fragment of apparent deglacial age in the same specimen, is as low as 13 mmol/mol (Fig. 8). The two Mg/Ca laser ablation scans presented in Fig. 8 show little variability within internal, visibly homogeneous, domains. Other minor and trace element to calcium ratios are presented alongside the laser ablation Mg/Ca ratio in Fig. 8 to better illustrate the properties of this high-Mg biogenic calcite. Note that ratios including elements measured close to or at the detection limit of the Thermo-Finnigan Element2 (e.g., Mn, U, Th) serve only to illustrate fine-scale Fe-Mn oxide impurities within the calcite.

Temporal changes in solution-based Mg/Ca ratios of the *Coralliidae* from the Amundsen Sea are shown with the Antarctic air temperature (δD) record from EPICA Dome C (Fig. 9). Since the internal section of *PS69/321-1-2*, which is the only coral fragment with a significantly reduced apparently deglacial Mg/Ca ratio and shows clear signs of dissolution, its distinctly lower Mg/Ca is not further discussed. As illustrated in Figure 9, specimens dating back to the middle of Marine Isotope Stage (MIS) 3 are systematically lower in Mg/Ca than their Holocene counterparts. Direct comparison of Mg/Ca with the Sr/Ca, even including the MIS 3 corals, shows no clear systematic trends (Fig. 10a), whereas slightly lower Mg/Ca in MIS 3 corals are associated with lower Ba/Ca (Fig. 10b). Coupled Mg/Ca and Li/Ca (hence Mg/Li) relationships were recently suggested to vary with calcification temperature in benthic foraminifera (Bryan and Marchitto, 2008) and cold-water scleractinia (Case et al., 2010; Raddatz et al., in press). These ratios are shown for the Amundsen Sea corals (Fig. 10c and d) with associated trendlines displayed for all data (grey) or only for those of corals of apparent late deglacial to Holocene age (black). While the R^2 including all data points is <0.4, and thus suggests no significant correlation, R^2 from corals younger than ~13 ka is >0.5, and therefore suggests some degree of correlation. Given rare glacial deep ocean temperature reconstructions (Adkins et al., 2002) the temperature range experienced by the cold-water corals from the Marie Byrd Seamounts during the late deglacial and Holocene was probably ≤2 °C in total, preventing a thorough assessment of temperature related changes in Mg/Ca ratios (see discussion below).

Interestingly, several of the *Coralliidae* investigated here have Mg/Li that are identical with, or higher than, seawater (open seawater at 35‰ psu: Mg/Li = 2.17 mol/mmol) (Angino and Billings, 1966; Culkin and Cox, 1966). The corals under investigation have Mg/Li ratios an order of magnitude higher than those reported by Case et al. (2010) or Raddatz et al. (in

press) for scleractinian cold water corals. Similarly depleted Mg/Li were reported for benthic foraminifera by Bryan and Marchitto (2008).

4. Discussion

4.1 Conversion of Amundsen coral conventional radiocarbon- into calendar ages

As shown in sections 3.2 and 4.2 (below), reliable U-series ages for early Holocene or older octocorals presented in this study cannot be provided. Nevertheless, it is possible to obtain approximate calendar ages based on conventional radiocarbon ages corrected by the likely local radiocarbon reservoir effect for a given time, derived from well-dated fossil corals collected in or close to the Drake Passage (Goldstein et al., 2001; Robinson and van de Flierdt, 2009; Burke and Robinson, 2012). Even though age information cannot be provided at centennial accuracy, such radiocarbon-based age information is still important for understanding the broad temporal growth patterns of these cold-water corals. Given that (i) the modern corals from the Amundsen Sea reproduce the modern radiocarbon reservoir effect, and (ii) very consistent radiocarbon age patterns were obtained for samples *PS69/318-1-4* and *PS69/321-1-2*, the radiocarbon age information obtained from the fossil octocorals is highly likely to be accurate.

Below the influence of nuclear bomb testing-derived radiocarbon (i.e., below water depths of ~800-1000m) (Sikes et al., 2008; Jenkins et al., 2010) the present-day CDW $\Delta^{14}C$ is homogenous in the Pacific sector of the Southern Ocean. According to GLODAP data, the modern $\Delta^{14}C$ between 1400 m and 3500 m water depth within CDW at the Drake Passage is almost identical with that for CDW in the Amundsen Sea, deviating by $\leq$2 ‰. However, during past climatic extremes, such as the LGM or Heinrich stadials, the oceanic radiocarbon inventory in the intermediate and deep Southern Ocean may have differed from today due to

changes in ventilation caused by shifts in the regional circulation regime (e.g., Robinson & van de Flierdt, 2009; Skinner et al. 2010). Although temporally variable, we regard the intermediate water depth Drake Passage and Amundsen Sea radiocarbon reservoir effect as comparable since both locations were bathed by CDW during the last glacial cycle.

Several studies have presented intermediate water radiocarbon reservoir ages for the Southern Ocean or Drake Passage for the last glacial-interglacial transition. Hall et al. (2010) showed that the Southern Ocean reservoir effect has not differed significantly from the modern situation in the Ross Sea shelf region throughout the last 6000 years. Intermediate water $\Delta^{14}C$ in the Drake Passage, corresponding to either CDW or Antarctic Intermediate Water, displays some scatter in radiocarbon offsets ($\Delta\Delta^{14}C$) from the contemporaneous ambient atmosphere over the past 15 ka, but likely had close to modern intermediate water radiocarbon concentrations during the latter part of the deglaciation after 15 ka (Burke and Robinson, 2012).

Estimating changes in the radiocarbon reservoir effect of Southern Ocean deep-water masses before the ACR is more difficult, but all available information hints at larger ambient $\Delta\Delta^{14}C$. The radiocarbon reservoir effect during the early deglaciation was approximately a third higher than the modern radiocarbon reservoir effect (Goldstein et al., 2001; Robinson and van de Flierdt, 2009; Burke and Robinson, 2012). Similarly depleted ambient radiocarbon reservoir effects are expected for intermediate Southern Ocean waters during fully glacial stages, though the only record available extends back only to Heinrich Stadial 2 (Burke and Robinson, 2012).

Geochemical and isotopic Amundsen Sea scleraxonian cold-water coral study

Given the above information, correcting the radiocarbon dates of corals from the Amundsen Sea that are younger than 15 ^{14}C ka BP by subtracting a radiocarbon reservoir effect equal to modern appears reasonable (Table 2, Fig. 3). However, several corals have conventional radiocarbon ages as old as 37.5 to 48.8 ^{14}C ka (Table 2). To date, no information exists on the CDW radiocarbon reservoir during MIS 3, but it was probably lower than during the LGM and the last deglaciation. Calendar ages in Table 2 are therefore calculated using a radiocarbon reservoir effect of 2000 years (1.43 times higher than modern) and 2500 (1.8 times higher than modern). We hypothesise that during MIS 3 the radiocarbon reservoir effect applicable to our coral samples was close to 2 ka (i.e., the local radiocarbon depletion relative to ambient atmosphere did not exceed that in Drake Passage intermediate waters at the LGM). Calibrated ages using this preferred radiocarbon reservoir effect define two populations, scattering around 41 ka and 49 ka. Apparently, no corals of MIS 2, LGM or early deglacial age were recovered (Table 2, Fig. 3), which may indicate unfavourable life conditions at intermediate water depths during this period (e.g. Thatje et al., 2005). For comparison, Robinson et al. (2007) report the widespread occurrence of cold-water scleractinia in the North Atlantic during the early deglaciation, an interval from which not a single specimen could be retrieved in the Marie Byrd Seamounts area.

4.2 U-series dating of calcitic cold-water corals

The U-Th disequilibrium dating approach has revealed unreliable fossil U-series ages for this family of *Coralliidae*. While recent and sub-recent fossil corals provide relatively realistic ages, most corals of more than a few thousand years in age clearly suffered from mobility and open system behaviour of uranium. In order to illustrate these U-series age artefacts, the results for two coral specimens sampled multiple times at high spatial resolution are shown in

Figs. 5 and 6. Since multiple reliable radiocarbon ages have been obtained (see section 4.1) independent age information is available for these specimens.

Coral *PS69/318-1-4* (Fig. 5) has an average radiocarbon-based calendar age of 12.6 cal ka BP, whereas its U-series ages range from ~9 to 76 ka. In the section of this coral shown in Fig. 5a all U-series ages are younger than the calibrated ^{14}C age (n=8), whereas those in the section in Fig. 5b are older (n=6). These two sections were taken less than 10 cm apart within the same coral branch, and the ^{14}C ages between these sections are indistinguishable within error.

Sample *PS69/321-1-2* contains an inner section formed approximately during the ACR at ~14 cal ka BP (Table 2) as well as an outer portion formed during the Holocene at ~6.3 cal ka BP (Fig. 6, Table 2). Both younger and older U-series ages were obtained for the Holocene section of this specimen, ranging from ~2.6 – 13.2 ka in sections without visible bioerosion (Fig. 6). This coral section also provides U-series data for a portion of coral with endolithic borings, demonstrating the effect of post-mortem bioerosion on the U-Th isotope systematics (*PS69/321-1-2-3a*, lower right of Fig. 6). The apparent U-series ages in this bioeroded zone are systematically older due to elevated $^{230}Th/^{238}U$ (see also Fig. 7). Although ^{230}Th appears significantly elevated, ^{232}Th concentrations are within the range of other coral samples (Fig. 7b, c). The deglacial inner section of coral *PS69/321-1-2* contains both highly elevated [^{232}Th] and $(^{230}Th/^{238}U)_{ACT}$ (Table 3), significantly outside the datable range for U-Th disequilibrium dating.

Based on the bulk coral sample results, and the additional high-resolution sampling of these two specimens, we identify several manifestations of open system-type behaviour in our

uranium series data. These include: (1) generally elevated $\delta^{234}U$ above seawater compositions; (2) uranium series ages that are younger than paired ^{14}C ages, with relatively standard initial $^{232}Th/^{230}Th$ ratios and low [^{232}Th]; (3) uranium series ages that are older than paired ^{14}C ages, with relatively standard $^{232}Th/^{230}Th$ ratios and elevated [^{232}Th]; (4) variable $^{232}Th/^{230}Th$ ratios in high-[^{232}Th] specimens, such that correction for initial ^{230}Th using the measured ^{232}Th removes all the ^{230}Th from the coral, hence over-correcting for the presence of initial ^{230}Th. Below we examine the processes that may cause these observations.

4.2.1 Addition of alpha-recoiled ^{234}U

Firstly, the most striking feature of the dataset is the generally elevated coral $\delta^{234}U$. Almost every fossil sample has $\delta^{234}U$ higher than present-day seawater $\delta^{234}U$ (Table 3, Fig. 4a). Without secular change in the seawater $\delta^{234}U$, post-mortem preferential addition of ^{234}U, or significant fine-scale sampling bias (Robinson et al. 2006), such a feature is physically impossible. Some authors have argued that the deglacial seawater $\delta^{234}U$ was higher than today following generally lower fully glacial $\delta^{234}U$ (Esat and Yokoyama, 2006; Esat and Yokoyama, 2010) and we need first to fully exclude this possibility. To better identify the underlying cause of elevated $\delta^{234}U$ in the fossil coral material, coral *PS69/318-1-4* has been sampled with a micro mill device covering the first few mm inward from the outer rim (Fig. 11). Results from the outermost sampled coral calcite define a $\delta^{234}U$ gradient of 51 ‰ over 2 mm, the outermost section being most enriched in ^{234}U ($\delta^{234}U$=196 ‰), therefore providing compelling evidence for diagenetic addition of ^{234}U rather than an initially elevated value. Hence while we acknowledge that glacial or deglacial seawater $\delta^{234}U$ may have been different from modern, the micro mill results suggest that the high present-day $\delta^{234}U$ found in these corals are controlled by diagenesis.

Preferential ^{234}U diffusion into corals has been observed and modeled in earlier studies. For example, in order to test the primary $^{234}U/^{238}U$ distribution in cold-water scleractinia, Robinson et al. (2006) tested the effect of various post-mortem processes in altering the coral $^{234}U/^{238}U$. Of all potentially important processes, these authors could identify alpha-recoil diffusion as the most effective. In brief, alpha-recoiled ^{234}U is hexavalent (Regil et al., 1989) and thus readily mobilised, after production, as a uranyl complex in oxic fluids. Fossil corals investigated here are typically coated with Fe-Mn oxides precipitated from the water column. Uranium concentrations in these Fe-Mn oxides were not determined here, but are likely comparable to concentrations observed in hydrogenetic ferromanganese crusts. Hence they should range from 7 to 16 μg/g U (Hein et al., 1999), approximately 65 to 150 times higher than [U] (on average 106 ng/g; Table 3) in these corals. Ejection of ^{234}U from these Fe-Mn oxides during alpha decay provides a source of excess ^{234}U that would then diffuse into fossil corals. This will be particularly pronounced given the low U concentrations in these octocorals (<250 ppb, as opposed to 1.5-4.5 ppm in the aragonitic corals studied by Robinson et al. 2006) and the large U concentration gradient that thus exists between Fe-Mn oxide coatings and coral calcite.

4.2.2 Isotopically variable initial $^{232}Th/^{230}Th$

In some samples elevated $^{230}Th/^{238}U$ was observed alongside elevated [^{232}Th] that cannot be adequately accounted for by typical initial seawater $^{232}Th/^{230}Th$. The fossil coral samples shown in Table 3 have been corrected for initial ^{230}Th using the most realistic (and previously used) water column $^{232}Th/^{230}Th$ for CDW in 1-2 km water depth (i.e., an atomic ratio of 5,000; see section 2.2) (cf., Goldstein et al., 2001; Burke and Robinson, 2012). While such a relatively low $^{232}Th/^{230}Th$ appears realistic for most fossil corals, two specimens required higher initial $^{232}Th/^{230}Th$ in order to avoid over-correction. The resulting U-series ages of

these two specimens are clearly arbitrary due to the choice of initial $^{232}Th/^{230}Th$ of 10,000 (see methods) but help to illustrate the effect of variable initial $^{232}Th/^{230}Th$. Also, in contrast to most fossil corals, the two modern specimens suggest initial $^{232}Th/^{230}Th$ for the modern sub-samples that are much higher and hence closer to average crustal compositions (section 3.2). Highly variable initial $^{232}Th/^{230}Th$ in fossil cold-water corals have previously been observed in aragonitic cold water corals (Cheng et al., 2000). The apparent high variability seen in the Amundsen Sea corals is attributed to isotopically variable Th supply through the water column, which may be a function of the Marie Byrd Seamounts location in the southernmost flow band of the Antarctic Circumpolar Current, in close proximity to the Antarctic continent (a viable source of ^{232}Th). We speculate that the occasional supply of small clay particles through the water column would suffice to create such $^{232}Th/^{230}Th$ variability. In the absence of these clay particles ambient CDW $^{232}Th/^{230}Th$ will be recorded, while the occasional presence of clays would significantly elevate the initial $^{232}Th/^{230}Th$. Since overall U, and therefore ^{230}Th concentrations, are low in Amundsen Sea *Coralliidae*, calculated U-series ages are very sensitive to inaccurate initial $^{232}Th/^{230}Th$ corrections.

4.2.3. Combined effect of U diffusion and isotopically variable initial $^{232}Th/^{230}Th$

Thorium is a highly particle-reactive element and thus will not diffuse easily within the calcite matrix (Langmuir and Herman, 1980; Scholz et al., 2004). Therefore age offsets due to open system behaviour observed in fossil Amundsen Sea corals will be controlled by uranium (not thorium) loss or uptake. This effect, as mentioned above, will be further offset by variable initial $^{232}Th/^{230}Th$.

Independent reliable ^{14}C age constraints are available for samples *PS69/318-1-4* and *PS69/321-1-2* (see section 4.1), allowing calculation of the expected in situ produced [^{230}Th]

based on the coral [^{238}U] and initial seawater (^{234}U/^{238}U)$_{ACT}$ of 1.1468. Comparing this calculated [^{230}Th] to the measured [^{230}Th] enables the quantification of U loss or uptake. If a sample contains more (less) ^{230}Th than expected, this provides strong support for uranium loss (gain) in individual coral sections. Besides the calculation of expected versus observed [^{230}Th], the difference between the apparent U-series and calibrated radiocarbon age can be determined for every sub-sample. A graphic illustration of these calculations is shown in Fig. 12. Both corals mapped for their U/Th isotope systematics show an increasing U-series age offset that directly depends on (i) U-loss or uptake and (ii) inadequate initial ^{230}Th correction.

While sample *PS69/318-1-4* shows a very clear exponential increase in the age offset corresponding to increasing uranium deficit (^{230}Th surplus), this relationship is not observed in sample *PS69/321-1-2* (Fig. 12). All but one coral sub-section shown in Fig. 12a with higher [^{230}Th] than expected (calculated [^{230}Th]/ measured [^{230}Th] < 1) have apparent U-series ages that are older than the calibrated radiocarbon age. Since [^{232}Th] is significantly elevated in every coral sub-sample with apparent U-series ages that are too old (Fig 12c, Table 3), the main factor producing overestimated U-series ages presented in Table 3 and Fig. 12 can be identified in the use of inappropriate initial ^{232}Th/^{230}Th for correction of non-decay-related ^{230}Th. For example, subtraction of typical crustal ^{232}Th/^{230}Th ratios to correct for the in situ produced ^{230}Th produces extremely old U-series ages (Fig. 13a). Typical Drake Passage intermediate water ^{232}Th/^{230}Th (5,000) (Goldstein et al., 2001; Burke and Robinson, 2012) also produces unsatisfactory U-series ages (Fig. 13a). A local initial ^{232}Th/^{230}Th of 2,000 for coral *PS69/318-1-4* produced U-series ages that are closest to the calibrated radiocarbon age of the same coral. Strikingly however, even this best-fit estimate for the initial ^{232}Th/^{230}Th for this particular coral specimen still resulted in U-series ages that are significantly offset from the calibrated radiocarbon age (Fig. 13b). Hence the age offset seen

in coral *PS69/318-1-4* can only be changed in amplitude, but not completely removed by altering the initial $^{232}Th/^{230}Th$, suggesting that the calculated offsets seen here must be caused by *combined* uranium loss/exchange and inaccurate initial [^{230}Th] correction.

Further, while *PS69/318-1-4* shows clear increasing age offsets with increasing amounts of initial Th (Fig. 12a), this relationship is not as simple for coral *PS69/321-1-2*. In fact, sample *PS69/321-1-2-3C* has an equally elevated [^{232}Th] compared with other samples displayed in Fig. 12, but a U-series age that is significantly too young (*PS69/321-1-2-3C*). Since U concentrations in this sample are comparable to surrounding sub-sections, this finding suggests isotopically inhomogenous incorporation of water-column-derived initial Th.

4.2.4 Non-alpha-recoil-related U mobility

Evidence for uranium gain can also be resolved. While many of the sub-sections shown in Fig. 12 contain more ^{230}Th than expected, several samples contain less ((calc. [^{230}Th]/ meas. [^{230}Th]) > 1; Fig. 12b). Since thorium is immobile in calcite this feature has to be ascribed to uranium-gain.

Non-alpha-decay-related uranium mobility in calcite has in fact been predicted before through XAFS and luminescence studies (Reeder et al., 2000). As stated above in the context of alpha-recoil ^{234}U diffusion, the oxidation state of U in aqueous solutions is 6+ and the dominant aqueous speciation involves the uranyl moiety (UO_2^{2+}). The dominant configuration in oxidising aqueous solutions, a uranyl tricarbonate ion, readily fits into the aragonite lattice but not into a calcite matrix (Reeder et al., 2000), leading to significant local disruption of the calcite structure, in turn raising concerns about its long-term retention. This structural constraint also explains the overall significantly lower U concentrations in calcite

reported here compared with aragonitic corals. Besides these structural considerations (Reeder et al., 2000), uranium addition into some fossil coral sections shown in Table 3 is also corroborated by elevated [^{238}U] in some of the fossil corals (as high as 268 ng/g) compared with the (sub-)modern corals [^{238}U] (25-55 ng/g). Hence, besides alpha-recoil-related ^{234}U diffusion into the corals, non-U-series-decay-related U diffusion within or into the coral is evident.

In summary, the octocorals of the family *Coralliidae* presented here: (i) undergo preferential alpha-recoil-related ^{234}U addition from enclosing Fe-Mn oxides into the calcite skeleton; (ii) sometimes contain elevated initial ^{230}Th, which cannot be properly accounted for due to variable initial ^{232}Th/^{230}Th; (iii) show significant simultaneous post-mortem diagenetic uranium (^{238}U) diffusion. Conversely, it should also be mentioned that one coral (*PS69/320-1-1*) has a calibrated radiocarbon age (~49 ka) that agrees remarkably well with the U-series age ($\Delta T \leq 1$ ka) (Table 3) despite present-day coral δ^{234}U of 179 ‰ and 185 ‰. For various reasons discussed above we conclude that this match is most likely coincidence.

4.3 The Mg/Ca ratio of Amundsen Sea octocorals – a potential proxy for CDW temperature?

Numerous studies have established Mg/Ca in benthic foraminifera as a proxy for ocean water temperature (e.g., Rosenthal et al., 1997; Lear et al., 2002; Elderfield et al., 2006). In contrast, only a few studies have investigated the elemental variability and distribution of Mg/Ca in corals with the particular aim to test their potential for palaeo-temperature reconstructions. Internally highly variable Mg/Ca ratios, which were reported from both zooxanthellate and azooxanthellate scleractinian cold-water corals (Gagnon et al., 2007; Meibom et al., 2008; Cohen et al., 2009; Case et al., 2010; Gaetani et al., 2011; Raddatz et al., in press), were

ascribed to strong biological mediation during calcification. The most extreme elemental fractionation effects during coral growth seem to depend on whether calcite was formed within early mineralisation zones (also known as centres of calcification), or within surrounding domains of fibrous aragonite (cf., Cuif and Dauphin, 2005). Usually, the internal variability in Mg/Ca observed in scleractinia is not primarily controlled by ambient water temperatures.

Studies investigating Mg/Ca ratios in coral species identical to those from the Amundsen Sea have not been carried out to date. Moreover, only a few papers have presented Mg/Ca ratios in calcitic octocorals of the genus *Corallium* spp. or *Paracorallium* spp. Results from the few existing non-scleractinian records suggest that calcitic octocorals have significantly higher Mg/Ca ratios (Weinbauer et al., 2000; Bond et al., 2005; Sherwood et al., 2005) than scleractinian cold-water corals or foraminifera. Critically, octocorals appear to be more promising archives than scleractinia in terms of recording ambient water temperatures with Mg/Ca (Bond et al., 2005; Sherwood et al., 2005).

Compared with aragonitic scleractinia, calcitic cold-water octocorals possibly use a different calcification mechanism. Given growth rates as low as a few tens of micrometres per year for certain *Coralliidae* (Roark et al., 2009), the skeletons of such slow-growing corals may be closer to chemical equilibrium with ambient water, and/or biological modification during calcification may be less extreme, or internal heterogeneities may be too small to be detected by conventional sampling strategies. The Mg/Ca ratio in our cold-water corals is strikingly homogeneous and highly elevated (Figure 8). The Mg/Ca ratios lie within the range of those from other octocorals (see below), which are an order of magnitude higher than Mg/Ca ratios reported for many benthic or planktic foraminifera. This apparent homogeneity within the

corals does not exclude the existence of small centres of calcification. Fallon et al. (2007) found evidence for sub-micrometre scale variability of Mg/Ca ratios in the calcitic coral species *Corallium secundum*, with Mg/Ca ratios being locally ≤40% higher than in the surrounding area. Hence although our coral laser ablation scans suggest homogeneity, this may simply be a smoothing effect because of the laser ablation spot size of 130 μm.

Of course, carbonate Mg/Ca ratios in our corals will likely be dependent on parameters other than ambient temperature. One diagnostic tool to assess biogeochemical modification within the calcifying compartment is the comparison of coral Mg/Ca to inorganically precipitated Mg/Ca in seawater for a given temperature. Oomuri et al. (1987) conducted extensive experiments to determine the temperature-dependent distribution coefficient (λ_{Mg}) in inorganic calcite. Their calibration covered temperatures from 10 to 50°C with various Mg/Ca in parent solutions, and suggested a linear dependence of λ_{Mg} on temperature. This calibration suggests a Mg/Ca of inorganically precipitated calcite, at ambient modern CDW temperatures (0.9°C) and typical seawater salinities, on the order of 25.4 mmol/mol. Modern coral sample *PS75/247-2-modern*, however, has a significantly higher Mg/Ca ratio of 78 mmol/mol, suggesting local biological modification at the calcification site. Hence, although internally relatively homogeneous, biological fractionation in the octocorals from the Marie Byrd Seamounts seems to elevate their Mg/Ca ratios relative to those expected for inorganic calcification.

Overall, it is impossible to provide a temperature calibration for the *Corrallidea* investigated here. More than one sampling location with differing temperature, salinity and carbonate ion concentrations would need to be included for a thorough calibration. On the Marie Byrd Seamounts, the modern water temperature ranges from 0.91°C at 1500 m water depth to

0.48°C at 2500 m water depth. Estimated glacial-interglacial temperature changes in the deep Southern Ocean are on the order of 1.5 to 3°C (Adkins et al., 2002; Elderfield et al., 2010). Most corals from the Amundsen Sea are either of late deglacial or Holocene age, so that they grew in waters that were already substantially warmer than at the LGM, i.e. these corals probably experienced a temperature change of less than 2°C. The early Holocene Mg/Ca ratios seem to be higher than the recent ones (Fig. 9). Late deglacial corals tend to have lower Mg/Ca ratios and MIS 3 corals display the lowest Mg/Ca ratios. Considering global climate change since MIS 3, these Mg/Ca trends can be expected, but identical corals sampled at different locations will be needed to corroborate them and to quantify their temperature significance.

At least for the late deglacial and Holocene corals shown in Figure 10, the degree of correlation between Mg/Ca and Li/Ca or Mg/Li ratios suggests that temperature probably has a systematic effect on the coral calcite Mg and Li, implying that both elements may be fractionated to varying degrees during incorporation into the coral calcite, depending on the same biogenic and physical controls. Given the inherent complexities of empirical Mg/Ca calibrations usually observed in marine biogenic carbonates (e.g., Elderfield et al., 2006; Gagnon et al., 2007; Meibom et al., 2008; Case et al., 2010; Gaetani et al., 2011) and the expected small temperature changes experienced at intermediate water depth in the Amundsen Sea since the final phase of the last deglaciation, the tentative correlation of Mg/Ca with Li/Ca ratios is an encouraging observation. Finally, we want to reiterate that although our coral Mg/Ca are apparently significantly elevated compared with expected inorganic Mg/Ca for given ambient seawater temperatures, the Mg/Li ratios of our *Coralliidae* match the seawater composition better than benthic foraminifera (Bryan and

Marchitto, 2008) or scleractinian cold-water corals (Case et al., 2010; Raddatz et al., in press).

5. Conclusions

Calcitic octocorals of the family *Coralliidae* collected in the Amundsen Sea are unsuitable for U-Th disequilibrium dating, largely because of uranium concentrations below 250 ng/g, uranium open system behaviour and isotopically variable initial Th. The low uranium concentration magnifies diagenetic artefacts caused by alpha-recoiled dissolved (as opposed to lattice-bound) ^{234}U diffusion into the coral, and was clearly resolved by means of micro-sampling of one coral of late deglacial ^{14}C age. Uranium loss and uptake lead to unpredictable offsets between U-series and ^{14}C ages. In contrast to aragonitic corals, diagenetic effects shown here are likely generic and will affect any calcitic cold-water coral, since incorporation of U distorts the calcite lattice (Reeder et al., 2000), and makes it prone to open system behaviour. Together with uranium mobility, isotopically (i.e., ^{232}Th/^{230}Th) highly variable initial Th at the studied site further makes adequate correction of non-in situ produced ^{230}Th impossible.

Radiocarbon contents of modern corals, on the other hand, match expected ambient CDW concentrations today, and fossil corals sampled multiple times for ^{14}C analyses produced very consistent conventional radiocarbon ages. Within a slightly expanded age uncertainty caused by uncertainty regarding the temporal variability of the local marine radiocarbon reservoir effect during growth, it is possible to obtain calibrated calendar ages for the corals from the Marie Byrd Seamounts. Most corals grew after 15 cal. ka BP, and no specimens were recovered from the early deglaciation, MIS 2 or late MIS 3. Several corals could be dated to approximately 40-49 cal. ka BP.

Geochemical and isotopic Amundsen Sea scleraxonian cold-water coral study

Laser ablation elemental mapping of the corals from the Amundsen Sea highlights differences in biomineralisation between these octocorals and the scleractinian aragonitic hexacorals more commonly used for paleoceanographic studies. The *Coralliidae* contain high-Mg calcite that is very homogeneous within individual growth domains. Features such as centres of calcification that find their expression in elevated Mg/Ca ratios compared to lower Mg/Ca ratios in surrounding fibrous aragonitic domains in scleractinia, are not visibly resolvable in laser ablation scans of these corals. Despite highly elevated Mg/Ca ratios, the internal homogeneity within single coral domains, as well as the tendency to slightly higher Mg/Ca ratios in late deglacial and Holocene corals compared to MIS 3, suggests that the Mg/Ca ratio responds to temperature, a feature that has previously been reported for other genus of octocorals. Since the expected ambient CDW water temperatures at intermediate depth during periods of coral growth probably varied by less than 2°C, a clear temperature dependence of the Mg/Ca ratio remains to be proven. Finally, coral Mg/Li are remarkably close to the seawater composition. In order to assess temperature effects or carbonate ion effects on the coral Mg/Ca or Mg/Li ratios for this genus, more samples from other localities need to be analysed.

Acknowledgements

The crews and the shipboard scientific parties during RV *Polarstern* expeditions (ANT-XXIII/4) in 2006 and (ANT-XXVI/3) in 2010, especially chief scientist Karsten Gohl, are thanked for all their help during coral sampling. Alistair Pike is thanked for providing access to the micromill within the Department of Archaeology and Anthropology at Bristol University. The analytical facilities of the Bristol Isotope Group would not work without the dedicated expertise of Chris Coath. Simon Powell (University of Bristol) helped with the

coral photographs shown in Fig 2. Morten Andersen and Eleni Anagnostou provided constructive suggestions during various discussions. Irka Hajdas is thanked for swift sample handling and radiocarbon measurements at ETH Zürich. Alex Rogers is acknowledged for advice on biological aspects of our coral collection. This research was funded by Leverhulme award F/00182/BQ to DV, and Marie Curie fellowship Project No. 220941 to MG. We appreciate and acknowledge constructive comments provided by two anonymous reviewers. Uwe Brand is thanked for editorial handling.

References

Adkins, J.F., Cheng, H., Boyle, E.A., Druffel, E.R.M., Edwards, R.L., 1998. Deep-sea coral evidence for rapid change in ventilation of the deep North Atlantic 15,400 years ago. Science, 280 (5364): 725-728.

Adkins, J.F., McIntyre, K., Schrag, D.P., 2002. The salinity, temperature, and delta O-18 of the glacial deep ocean. Science, 298 (5599): 1769-1773.

Andersen, M.B., Stirling, C.H., Potter, E.K., Halliday, A.N., Blake, S.G., McCulloch, M.T., Ayling, B.F., O'Leary, M., 2008. High-precision U-series measurements of more than 500,000 year old fossil corals. Earth and Planetary Science Letters, 265 (1-2): 229-245.

Andersen, M.B., Stirling, C.H., Zimmermann, B., Halliday, A.N., 2010. Precise determination of the open ocean 234U/238U composition. Geochemistry Geophysics Geosystems, 11 (12): Art. No.: Q12003.

Anderson, R.F., Ali, S., Bradtmiller, L.I., Nielsen, S.H.H., Fleisher, M.Q., Anderson, B.E., Burckle, L.H., 2009. Wind-driven upwelling in the Southern Ocean and the deglacial rise in atmospheric CO2. Science, 323 (5920): 1443-1448.

Angino, E.E., Billings, G.K., 1966. Lithium content of sea water by atomic absorption spectrometry. Geochimica et Cosmochimica Acta, 30 (2): 153-158.

Archer, D., Winguth, A., Lea, D., Mahowald, N., 2000. What caused the glacial/interglacial atmospheric pCO(2) cycles? Reviews of Geophysics, 38 (2): 159-189.

Berkman, P.A., Forman, S.L., 1996. Pre-bomb radiocarbon and the reservoir correction for calcareous marine species in the Southern Ocean. Geophysical Research Letters, 23 (4): 363-366.

Bond, Z.A., Cohen, A.L., Smith, S.R., Jenkins, W.J., 2005. Growth and composition of high-Mg calcite in the skeleton of a Bermudian gorgonian (Plexaurella dichotoma):

Potential for paleothermometry. Geochemistry Geophysics Geosystems, 6: Art. No.: Q08010.

Brovkin, V., Ganopolski, A., Archer, D., Rahmstorf, S., 2007. Lowering of glacial atmospheric CO2 in response to changes in oceanic circulation and marine biogeochemistry. Paleoceanography, 22: Art. No.: PA4202.

Bryan, S.P., Marchitto, T.M., 2008. Mg/Ca-temperature proxy in benthic foraminifera: New calibrations from the Florida Straits and a hypothesis regarding Mg/Li. Paleoceanography, 23 (2): Art. No.: PA2220.

Burke, A., Robinson, L.F., 2012. The Southern Ocean's role in carbon exchange during the last deglaciation. Science, 335 (6068): 557-561.

Case, D.H., Robinson, L.F., Auro, M.E., Gagnon, A.C., 2010. Environmental and biological controls on Mg and Li in deep-sea scleractinian corals. Earth and Planetary Science Letters, 300 (3-4): 215-225.

Chen, J.H., Lawrence Edwards, R., Wasserburg, G.J., 1986. U-238, U-234 and Th-232 in seawater. Earth and Planetary Science Letters, 80 (3-4): 241-251.

Cheng, H., Adkins, J., Edwards, R.L., Boyle, E.A., 2000. U-Th dating of deep-sea corals. Geochimica et Cosmochimica Acta, 64 (14): 2401-2416.

Cohen, A.L., McCorkle, D.C., de Putron, S., Gaetani, G.A., Rose, K.A., 2009. Morphological and compositional changes in the skeletons of new coral recruits reared in acidified seawater: Insights into the biomineralization response to ocean acidification. Geochemistry Geophysics Geosystems, 10: Art. No.: Q07005.

Cuif, J.-P., Dauphin, Y., 2005. The two-step mode of growth in the scleractinian coral skeletons from the micrometre to the overall scale. Journal of Structural Biology, 150 (3): 319-331.

Culkin, F., Cox, R.A., 1966. Sodium, potassium, magnesium, calcium and strontium in seawater. Deep Sea Research, 13 ((5)): 789-804.

Edwards, R.L., Chen, J.H., Wasserburg, G.J., 1987. U-238 U-234-Th-230-Th-232 systematics and the precise measurement of time over the past 500,000 years. Earth and Planetary Science Letters, 81 (2-3): 175-192.

Elderfield, H., Greaves, M., Barker, S., Hall, I.R., Tripati, A., Ferretti, P., Crowhurst, S., Booth, L., Daunt, C., 2010. A record of bottom water temperature and seawater delta(18)O for the Southern Ocean over the past 440 kyr based on Mg/Ca of benthic foraminiferal Uvigerina spp. Quaternary Science Reviews, 29 (1-2): 160-169.

Elderfield, H., Yu, J., Anand, P., Kiefer, T., Nyland, B., 2006. Calibrations for benthic foraminiferal Mg/Ca paleothermometry and the carbonate ion hypothesis. Earth and Planetary Science Letters, 250 (3-4): 633-649.

EPICA-Community-Members, 2004. Eight glacial cycles from an Antarctic ice core. Nature, 429 (6992): 623-628.

Esat, T.M., Yokoyama, Y., 2006. Variability in the uranium isotopic composition of the oceans over glacial-interglacial timescales. Geochimica et Cosmochimica Acta, 70 (16): 4140-4150.

Esat, T.M., Yokoyama, Y., 2010. Coupled uranium isotope and sea-level variations in the oceans. Geochimica et Cosmochimica Acta, 74 (24): 7008-7020.

Fairbanks, R.G., Mortlock, R.A., Chiu, T.C., Cao, L., Kaplan, A., Guilderson, T.P., Fairbanks, T.W., Bloom, A.L., Grootes, P.M., Nadeau, M.J., 2005. Radiocarbon calibration curve spanning 0 to 50,000 years BP based on paired Th-230/U-234/U-238 and C-14 dates on pristine corals. Quaternary Science Reviews, 24 (16-17): 1781-1796.

Fallon, S.J., Roark, E.B., Guilderson, T.P., Dunbar, R.B., Weber, P., 2007. Elemental Imaging and Proxy Development in the Deep Sea Corals. AGU Fall Meeting 2007 Conference Abstract: #PP42A-05.

Gaetani, G.A., Cohen, A.L., Wang, Z., Crusius, J., 2011. Rayleigh-based, multi-element coral thermometry: A biomineralization approach to developing climate proxies. Geochimica et Cosmochimica Acta, 75 (7): 1920-1932.

Gagnon, A.C., Adkins, J.F., Fernandez, D.P., Robinson, L.F., 2007. Sr/Ca and Mg/Ca vital effects correlated with skeletal architecture in a scleractinian deep-sea coral and the role of Rayleigh fractionation. Earth and Planetary Science Letters, 261 (1-2): 280-295.

Gohl, K., 2006. The Expedition ANT-XXIII/4 of the Research Vessel Polarstern in 2006, Alfred Wegener Institute for Polar and Marine Research, Bremerhaven.

Gohl, K., 2010. The Expedition of the Research Vessel "Polarstern" to the Amundsen Sea, Antarctica, in 2010 (ANT-XXVI/3), Alfred Wegener Institute for Polar and Marine Research, Bremerhaven.

Goldstein, S.J., Lea, D.W., Chakraborty, S., Kashgarian, M., Murrell, M.T., 2001. Uranium-series and radiocarbon geochronology of deep-sea corals: implications for Southern Ocean ventilation rates and the oceanic carbon cycle. Earth and Planetary Science Letters, 193 (1-2): 167-182.

Hajdas, I., Bonani, G., Thut, H., Leone, G., Pfenninger, R., Maden, C., 2004a. A report on sample preparation at the ETH/PSI AMS facility in Zurich. Nuclear Instruments & Methods in Physics Research Section B-Beam Interactions with Materials and Atoms, 223 267-271.

Hajdas, I., Bonani, G., Zimmerman, S.H., Mendelson, M., Hemming, S., 2004b. C-14 ages of ostracodes from pleistocene lake sediments of the western Great Basin, USA - results of progressive acid leaching. Radiocarbon, 46 (1): 189-200.

Hall, B.L., Henderson, G.M., Baroni, C., Kellogg, T.B., 2010. Constant Holocene Southern-Ocean C-14 reservoir ages and ice-shelf flow rates. Earth and Planetary Science Letters, 296 (1-2): 115-123.

Hein, J.R., Koschinsky, A., Bau, M., Manheim, F.T., Kang, J.-K., Roberts, L., 1999. Cobalt-rich ferromanganese crusts in the Pacific. In: Cronan, D.S. (Ed.), Handbook of marine mineral deposits. CRC Press, pp. 239-279.

Henderson, G.M., 2002. Seawater (U-234/U-238) during the last 800 thousand years. Earth and Planetary Science Letters, 199 (1-2): 97-110.

Hoffmann, D.L., Prytulak, J., Richards, D.A., Elliott, T., Coath, C.D., Smart, P.L., Scholz, D., 2007. Procedures for accurate U and Th isotope measurements by high precision MC-ICPMS. International Journal of Mass Spectrometry, 264 (2-3): 97-109.

Jenkins, W.J., Elder, K.L., McNichol, A.P., von Reden, K., 2010. The passage of the bomb radiocarbon pulse into the Pacific Ocean. Radiocarbon, 52 (3): 1182-1190.

Jochum, K.P., Weis, U., Stoll, B., Kuzmin, D., Yang, Q., Raczek, I., Jacob, D.E., Stracke, A., Birbaum, K., Frick, D.A., Günther, D., Enzweiler, J., 2011. Determination of Reference Values for NIST SRM 610–617 Glasses Following ISO Guidelines. Geostandards and Geoanalytical Research: 33 pages.

Langmuir, D., Herman, J.S., 1980. The mobility of thorium in natural waters at low temperatures. Geochimica et Cosmochimica Acta, 44 (11): 1753-1766.

Lear, C.H., Rosenthal, Y., Slowey, N., 2002. Benthic foraminiferal Mg/Ca-paleothermometry: A revised core-top calibration. Geochimica et Cosmochimica Acta, 66 (19): 3375-3387.

Lomitschka, M., Mangini, A., 1999. Precise Th/U-dating of small and heavily coated samples of deep sea corals. Earth and Planetary Science Letters, 170 (4): 391-401.

Ludwig, K.R., 2003. User's manual for Isoplot 3.00, a geochronological toolkit for Microsoft Excel, Berkeley Geochronology Center, Berkeley, U.S.A.

Luo, X.Z., Rehkamper, M., Lee, D.C., Halliday, A.N., 1997. High precision Th-230/Th-232 and U-234/U-238 measurements using energy-filtered ICP magnetic sector multiple collector mass spectrometry. International Journal of Mass Spectrometry, 171 (1-3): 105-117.

Mangini, A., Godoy, J.M., Godoy, M.L., Kowsmann, R., Santos, G.M., Ruckelshausen, M., Schroeder-Ritzrau, A., Wacker, L., 2010. Deep sea corals off Brazil verify a poorly ventilated Southern Pacific Ocean during H2, H1 and the Younger Dryas. Earth and Planetary Science Letters, 293 (3-4): 269-276.

Mangini, A., Lomitschka, M., Eichstadter, R., Frank, N., Vogler, S., Bonani, G., Hajdas, I., Patzold, J., 1998. Coral provides way to age deep water. Nature, 392 (6674): 347-348.

Marchitto, T.M., Lehman, S.J., Ortiz, J.D., Fluckiger, J., van Geen, A., 2007. Marine radiocarbon evidence for the mechanism of deglacial atmospheric CO2 rise. Science, 316 (5830): 1456-1459.

Matsumoto, A.K., 2007. Effects of low water temperature on growth and magnesium carbonate concentrations in the cold-water gorgonian Primnoa pacifica. Bulletin of Marine Science, 81 (3): 423-435.

Meibom, A., Cuif, J.-P., Houlbreque, F., Mostefaoui, S., Dauphin, Y., Meibom, K.L., Dunbar, R., 2008. Compositional variations at ultra-structure length scales in coral skeleton. Geochimica et Cosmochimica Acta, 72 (6): 1555-1569.

Nemec, M., Wacker, L., Gaeggeler, H., 2010. Optimization of the graphitization process at age-1. Radiocarbon, 52 (3): 1380-1393.

Oomori, T., Kaneshima, H., Maezato, Y., Kitano, Y., 1987. Distribution coefficient of Mg-2+ ions between calcite and solution at 10-50°C. Marine Chemistry, 20 (4): 327-336.

Pons-Branchu, E., Hillaire-Marcel, C., Deschamps, P., Ghaleb, B., Sinclair, D.J., 2005. Early diagenesis impact on precise U-series dating of deep-sea corals: Example of a 100-200-year old Lophelia pertusa sample from the Northeast Atlantic. Geochimica et Cosmochimica Acta, 69 (20): 4865-4879.

Raddatz, J., Liebetrau, V., Rüggeberg, A., Hathorne, E., Krabbenhöft, A., Eisenhauer, A., Böhm, F., Vollstaedt, H., Fietzke, J., López Correa, M., Freiwald, A., Dullo, W.C., in press. Stable Sr-isotope, Sr/Ca, Mg/Ca, Li/Ca and Mg/Li ratios in the scleractinian cold-water coral Lophelia pertusa. Chemical Geology.

Reeder, R.J., Nugent, M., Lamble, G.M., Tait, C.D., Morris, D.E., 2000. Uranyl incorporation into calcite and aragonite: XAFS and luminescence studies. Environ. Sci. Technol., 34: 638-644.

Regil, E.O., Schleiffer, J.J., Adloff, J.P., Roessler, K., 1989. Chemical effects of alpha-decay in uranium minerals. Radiochimica Acta, 47 (4): 177-185.

Roark, E.B., Guilderson, T.P., Dunbar, R.B., Fallon, S.J., Mucciarone, D.A., 2009. Extreme longevity in proteinaceous deep-sea corals. Proceedings of the National Academy of Sciences of the United States of America, 106 (13): 5204-5208.

Robinson, L.F., Adkins, J.F., Fernandez, D.P., Burnett, D.S., Wang, S.L., Gagnon, A.C., Krakauer, N., 2006. Primary U distribution in scleractinian corals and its implications for U series dating. Geochemistry Geophysics Geosystems, 7 Art. No.: Q05022.

Robinson, L.F., Adkins, J.F., Keigwin, L.D., Southon, J., Fernandez, D.P., Wang, S.L., Scheirer, D.S., 2005. Radiocarbon variability in the western North Atlantic during the last deglaciation. Science, 310 (5753): 1469-1473.

Robinson, L.F., Adkins, J.F., Scheirer, D.S., Fernandez, D.P., Gagnon, A., Waller, R.G., 2007. Deep-sea scleractinian coral age and depth distributions in the northwest Atlantic for the last 225,000 years. Bulletin of Marine Science, 81(3): 371-391.

Robinson, L.F., van de Flierdt, T., 2009. Southern Ocean evidence for reduced export of North Atlantic Deep Water during Heinrich Event 1. Geology, 37 (3): 195-198.

Rosenthal, Y., Boyle, E.A., Slowey, N., 1997. Temperature control on the incorporation of magnesium, strontium, fluorine, and cadmium into benthic foraminiferal shells from Little Bahama Bank: Prospects for thermocline paleoceanography. Geochimica et Cosmochimica Acta, 61 (17): 3633-3643.

Scholz, D., Mangini, A., 2007. How precise are U-series coral ages? Geochimica et Cosmochimica Acta, 71 (8): 1935-1948.

Scholz, D., Mangini, A., Felis, T., 2004. U-series dating of diagenetically altered fossil reef corals. Earth and Planetary Science Letters, 218 (1-2): 163-178.

Sherwood, O.A., Heikoop, J.M., Sinclair, D.J., Scott, D.B., Risk, M.J., Shearer, C., Azetsu-Scott, K., 2005. Skeletal Mg/Ca in Primnoa resedaeformis: relationship to temperature? Cold-Water Corals and Ecosystems, 1061-1079 pp.

Sikes, E.L., Burgess, S.N., Grandpre, R., Guilderson, T.P., 2008. Assessing modern deep-water ages in the New Zealand region using deep-water corals. Deep-Sea Research Part I, 55 (1): 38-49.

Sikes, E.L., Samson, C.R., Guilderson, T.P., Howard, W.R., 2000. Old radiocarbon ages in the southwest Pacific Ocean during the last glacial period and deglaciation. Nature, 405 (6786): 555-559.

Skinner, L.C., Fallon, S., Waelbroeck, C., Michel, E., Barker, S., 2010. Ventilation of the deep Southern Ocean and deglacial CO2 rise. Science, 328 (5982): 1147-1151.

Stenni, B., Buiron, D., Frezzotti, M., Albani, S., Barbante, C., Bard, E., Barnola, J.M., Baroni, M., Baumgartner, M., Bonazza, M., Capron, E., Castellano, E., Chappellaz, J., Delmonte, B., Falourd, S., Genoni, L., Iacumin, P., Jouzel, J., Kipfstuhl, S., Landais, A., Lemieux-Dudon, B., Maggi, V., Masson-Delmotte, V., Mazzola, C., Minster, B., Montagnat, M., Mulvaney, R., Narcisi, B., Oerter, H., Parrenin, F., Petit, J.R., Ritz, C., Scarchilli, C., Schilt, A., Schuepbach, S., Schwander, J., Selmo, E., Severi, M., Stocker, T.F., Udisti, R., 2011. Expression of the bipolar see-saw in Antarctic climate records during the last deglaciation. Nature Geoscience, 4 (1): 46-49.

Stirling, C.H., Andersen, M.B., 2009. Uranium-series dating of fossil coral reefs: Extending the sea-level record beyond the last glacial cycle. Earth and Planetary Science Letters, 284 (3-4): 269-283.

Thatje, S., Hillenbrand, C.D., Larter, R., 2005. On the origin of Antarctic marine benthic community structure. Trends in Ecology & Evolution, 20 (10): 534-540.

Toggweiler, J.R., Russell, J.L., Carson, S.R., 2006. Midlatitude westerlies, atmospheric CO2, and climate change during the ice ages. Paleoceanography, 21(2).

Wacker, L., Bonani, G., Friedrich, M., Hajdas, I., Kromer, B., Nemec, M., Ruff, M., Suter, M., Synal, H.A., Vockenhuber, C., 2010. MICADAS: Routine and high-precision radiocarbon dating. Radiocarbon, 52 (2): 252-262.

Weinbauer, M.G., Brandstätter, F., Velimirov, B., 2000. On the potential use of magnesium and strontium concentrations as ecological indicators in the calcite skeleton of the red coral (Corallium rubrum). Marine Biology, 137 (5): 801-809.

Figure Captions

Fig. 1. Cold-water coral sampling locations on the Marie Byrd Seamounts in the Amundsen Sea (Pacific sector of the Southern Ocean). Bathymetric map was generated using GMT.

Fig. 2. Two modern branches (left) and two fossil coral sections (right) of typical *Coralliidae* samples collected from the Marie Byrd Seamounts. Note the presence of two growth phases separated by an internal Fe-Mn layer within both fossil specimens. Such internal overgrowths were also observed in several other fossil coral samples. The Fe-Mn oxide layers are host to various particle-reactive trace metals that can affect the reliability of U/Th disequilibrium ages. Based on calibrated radiocarbon ages *PS69/325-1-1* grew at ~47 cal ka BP, while *PS75/250-1-1* dates back to approximately 11.2 cal ka BP (see Table 2).

Fig. 3. Fossil coral age distribution of analysed samples based on calibrated radiocarbon dates and a few late Holocene closed system U/Th ages. The Antarctic EPICA Dome C δD ice core record (EPICA-Community-Members, 2004) is shown for comparison, and to set the observed phases of coral growth in the Amundsen Sea in the context of climatic boundary conditions in Antarctica. A1-A3 refer to Antarctic warming phases.

Fig. 4. (A) Summary plot showing all U-Th cold-water coral data produced in the course of this study. The solid line indicates the closed system trajectory, along which $(^{234}U/^{238}U)_{ACT}$ and $(^{230}Th/^{238}U)_{ACT}$ should develop after coral death, starting with an initial seawater $(^{234}U/^{238}U)_{ACT}$ of 1.1468 (Andersen et al., 2010) and successively trending towards secular equilibrium values (=1), thereby also leading to an increase in $(^{230}Th/^{238}U)_{ACT}$ due to ingrowth of ^{230}Th from ^{234}U decay. White circles on the line highlight theoretical coral

$(^{234}U/^{238}U)_{ACT}$ and $(^{230}Th/^{238}U)_{ACT}$ in 20 ka intervals following death. Dashed grey lines delineate closed system U/Th isotopic evolution patterns for potential seawater $(^{234}U/^{238}U)_{ACT}$ of 1.15 and 1.16, suggested for the last deglaciation (cf., Esat and Yokoyama, 2006). **(B)** Uranium-thorium isotopic results for the two modern specimens shown in Fig. 2. Compositions of sample *PS69/319-1-modern* are shown with dotted lines, those of *PS75/247-2-modern* with solid lines. **(C)** High-resolution sampling of coral specimen *PS69/318-1-4*, which grew during the last deglaciation, and **(D)** individual results of similar high-resolution samples of coral *PS69/321-1-2*. Both corals show clear evidence for open system behaviour.

Fig. 5. Summary of high-resolution analyses of sample *PS69/318-1-4* showing individual conventional radiocarbon ages of coral sub-sections (centre), as well as calculated apparent U-series ages (left and right, bold font). These latter deviate substantially from the ^{14}C-derived coral ages. Further evidence of their unreliability is seen in the individual modern $(^{234}U/^{238}U)_{ACT}$ and initial $(^{234}U/^{238}U)_{ACT}$ (left and right, regular font beneath the calculated U-series age). The initial $(^{234}U/^{238}U)_{ACT}$ is determined for the calculated apparent coral U-series age. Strikingly, even the present-day $(^{234}U/^{238}U)_{ACT}$ are higher than present-day seawater $(^{234}U/^{238}U)_{ACT}$ of 1.1468 (Andersen et al., 2010) Note also the difference in calcite texture between the two coral sections figured in A versus B, sampled less than 10 cm apart within the same coral branch. The calibrated radiocarbon age (12.6 cal ka BP) given in the yellow plate is based on the average age of all radiocarbon sub-samples shown in panels (A) and (B).

Fig. 6. Summary of high-resolution analyses of sample *PS69/321-1-2* showing individual conventional radiocarbon ages (centre) of coral sub-sections as well as calculated apparent U-series ages (left and right, bold font). These latter deviate substantially from the ^{14}C-derived coral ages. Further evidence of their unreliability is seen in the individual modern

($^{234}U/^{238}U)_{ACT}$ and initial ($^{234}U/^{238}U)_{ACT}$ (left and right, regular font beneath the calculated U-series age). The initial ($^{234}U/^{238}U)_{ACT}$ is determined for the calculated apparent coral U-series age.The figured section contains an inner section of mid-deglacial age (~14 cal. ka BP) and an outer Holocene section (~6.27 cal. ka BP). The sub-samples on the lower right side were run in order to test the effect of endolithic borings in offsetting the coral U-series systematics. The U/Th isotopic compositions measured in the inner section suggest highly enriched [^{232}Th] and [^{230}Th] with compositions significantly outside the U-series disequilibrium dating range. Combined highly elevated ($^{234}U/^{238}U)_{ACT}$ and ($^{230}Th/^{238}U)_{ACT}$ cannot be reliably corrected for (c.f., Andersen et al., 2008).

Fig. 7. Relationship of **(A)** present-day coral δ^{234}U to the calculated apparent U-series ages, **(B)** [^{232}Th] compared with calculated apparent U-series ages, **(C)** [^{232}Th] versus the corrected ($^{230}Th/^{238}U)_{ACT}$ and **(D)** the measured ($^{232}Th/^{238}U)_{ACT}$ compared with the corrected ($^{230}Th/^{238}U)_{ACT}$. Coral specimens *PS69/314-1-4* and *PS69/231-1-2* are highlighted. Error bars in **(B)** to **(D)** are smaller than symbol sizes.

Fig. 8. Multi element laser ablation mapping results for two fossil octocorals. The left specimen (*PS69/321-1-2*) contains a section of mid-deglacial age overgrown by a Holocene outer part. Mn/Ca, U/Ca and Th/Ca ratios are only plotted to illustrate the effect of internal Fe-Mn oxide layers that also contain elevated Th concentrations.

Fig. 9. Fossil coral solution-based Mg/Ca records, set in relation to the Antarctic EPICA Dome C δD ice core record (EPICA-Community-Members, 2004). A proper temperature calibration for Mg/Ca cannot be provided here.

Fig. 10. Solution-based fossil coral multi element ratio plots. Trend lines and regression coefficients in **(C)** and **(D)** assess the degree of correlation for all samples (solid black line, black font) and for corals of deglacial to recent age (dotted grey line, grey font), respectively. See text for further discussion.

Fig. 11. Present-day $(^{234}U/^{238}U)_{ACT}$ of sample *PS69/318-1-4* analysed using a micro mill to detect $^{234}U/^{238}U$ gradients from the coral rim inwards. The $(^{234}U/^{238}U)_{ACT}$ along the outermost 2 mm changes by 0.051, corresponding to a gradient in $\delta^{234}U$ over this depth interval of 51 ‰. The white diamonds mark dated inner sections of this coral (shown in Fig. 8). Note that all sub-samples have higher than present-day seawater $(^{234}U/^{238}U)_{ACT}$ despite a coral age of 12.6 cal ka BP.

Fig. 12. Offsets of calculated U-series ages relative to the calibrated radiocarbon-derived calendar ages for coral samples *PS69/318-1-4* and *PS69/321-1-2* plotted versus the individual coral sub-sample U/Th budget **(A)**. Based on the coral U concentration of each individual sample and an initial seawater $(^{234}U/^{238}U)_{ACT}$, the theoretical amount of *in situ* produced [^{230}Th] since coral fossilisation can be calculated. Comparing this to the measured coral [^{230}Th] enables an assessment of whether, due to uranium mobility, a coral sub-sample contains more or less [^{230}Th] than expected and hence of its effect on the calculated offset of the U-series age from the most realistic (i.e. the calibrated radiocarbon) age. The largest offsets are recorded for samples containing substantial amounts of initial Th. However, some samples contain less ^{230}Th than expected, indicative of U gain **(B)**. These corals also produced younger-than-realistic U-series ages. **(C)** Offset of calculated U-series ages in relation to the coral $(^{232}Th/^{238}U)_{ACT}$. Larger offsets are accompanied by higher $(^{232}Th/^{238}U)_{ACT}$, yet the absolute age offset is variable.

Fig. 13. (A) Apparent U-series ages for sub-samples of coral *PS69/318-1-4* corrected for initial Th using: (1) an initial atomic $^{232}Th/^{230}Th$ 231,000 (typical crustal compositions); (2) 5,000 (analogous to Goldstein et al. (2001) and Burke and Robinson (2012)); and (3) 2,000 (best-fit initial ratio for this specimen). **(B)** The same coral samples shown in A but using an expanded vertical scale. Even with the most realistic initial $^{232}Th/^{230}Th$ the apparent U-series ages are significantly too old when compared to the corresponding radiocarbon date (see text for discussion), highlighting further offset caused by uranium mobility.

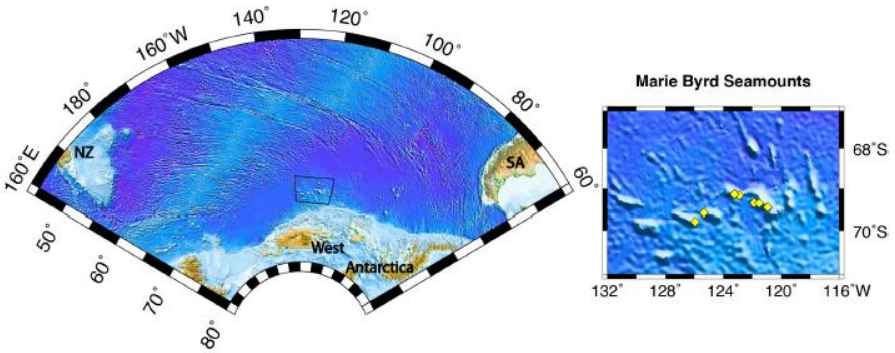

Figure 1.
Gutjahr et al.
Chemical Geology

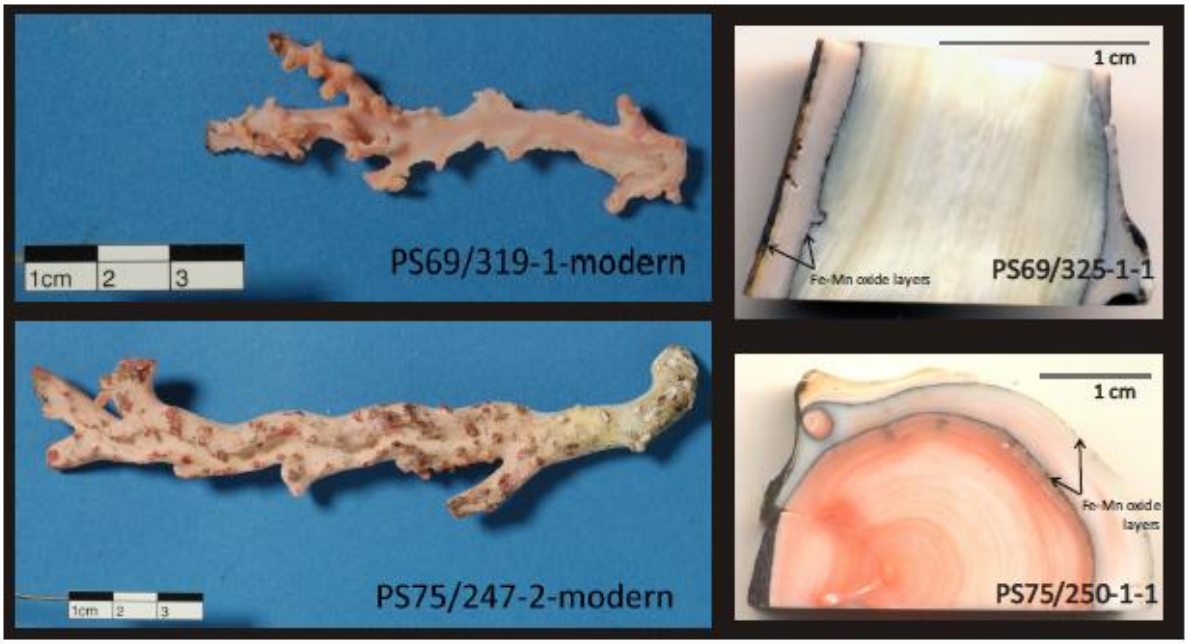

Figure 2.
Gutjahr et al.
Chemical Geology

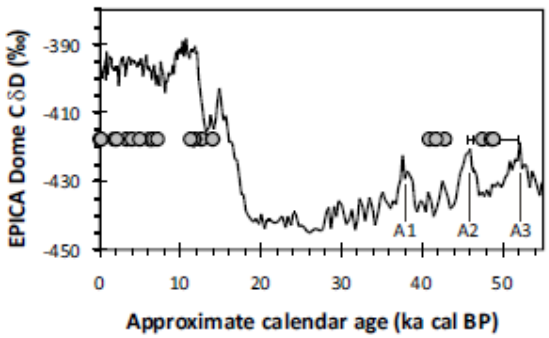

Figure 3.
Gutjahr et al.
Chemical Geology

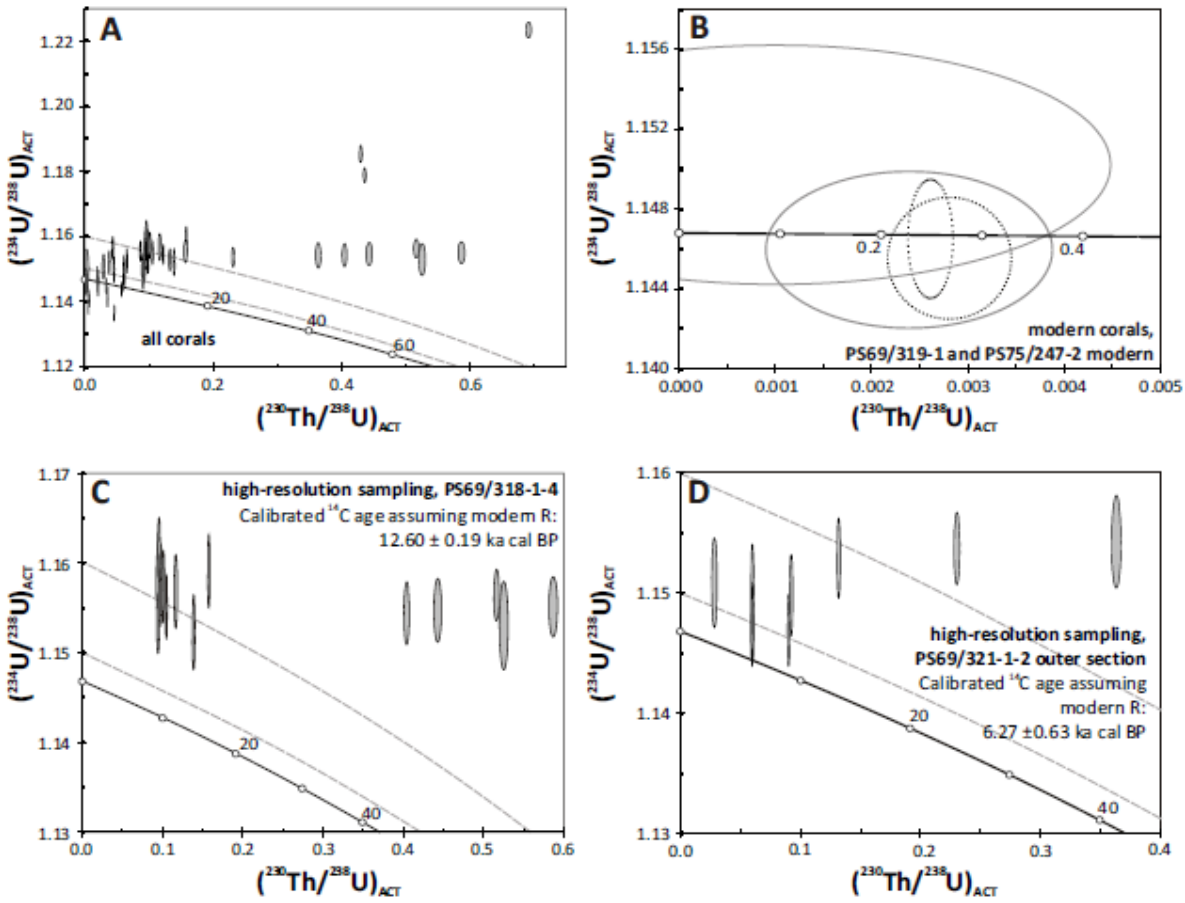

Figure 4.
Gutjahr et al.
Chemical Geology

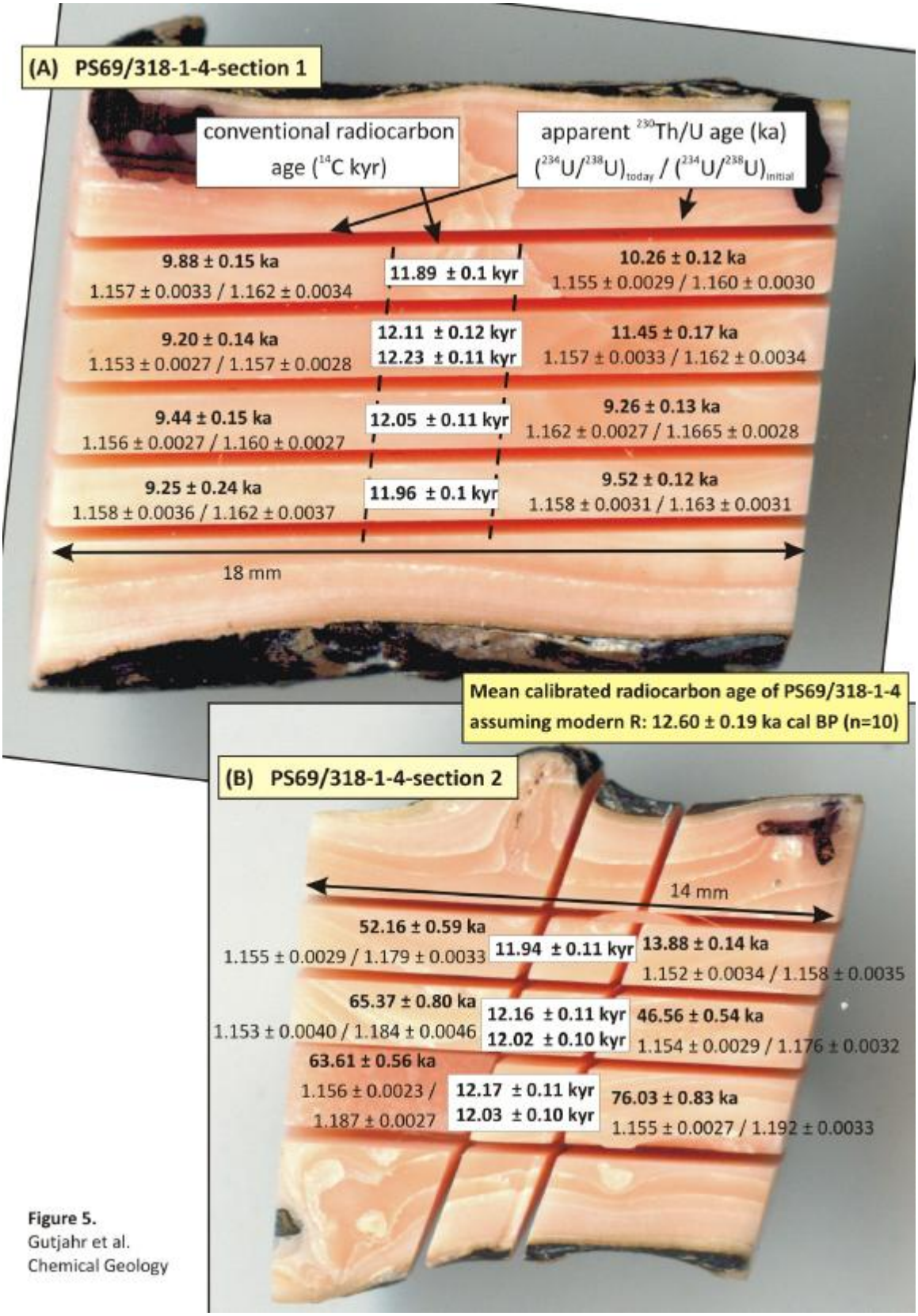

Figure 5.
Gutjahr et al.
Chemical Geology

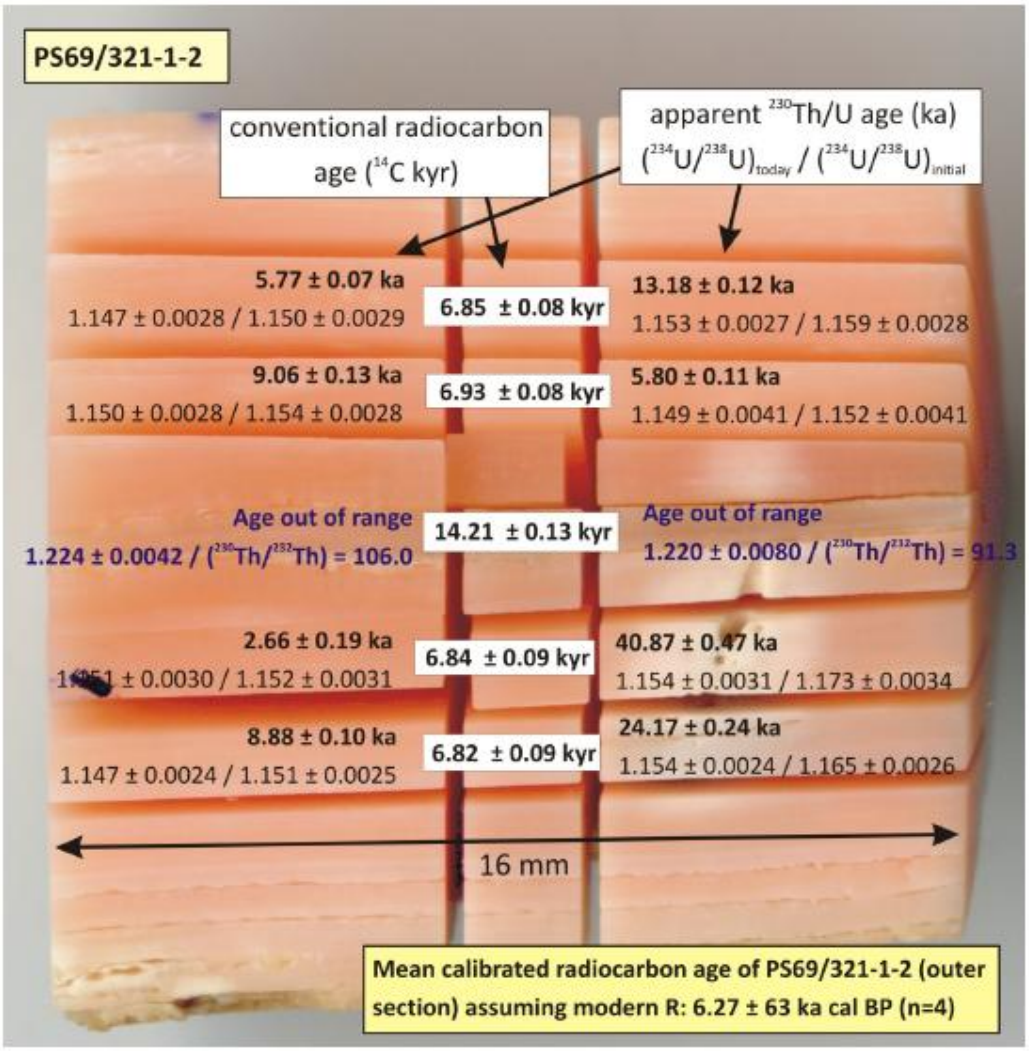

Figure 6.
Gutjahr et al.
Chemical Geology

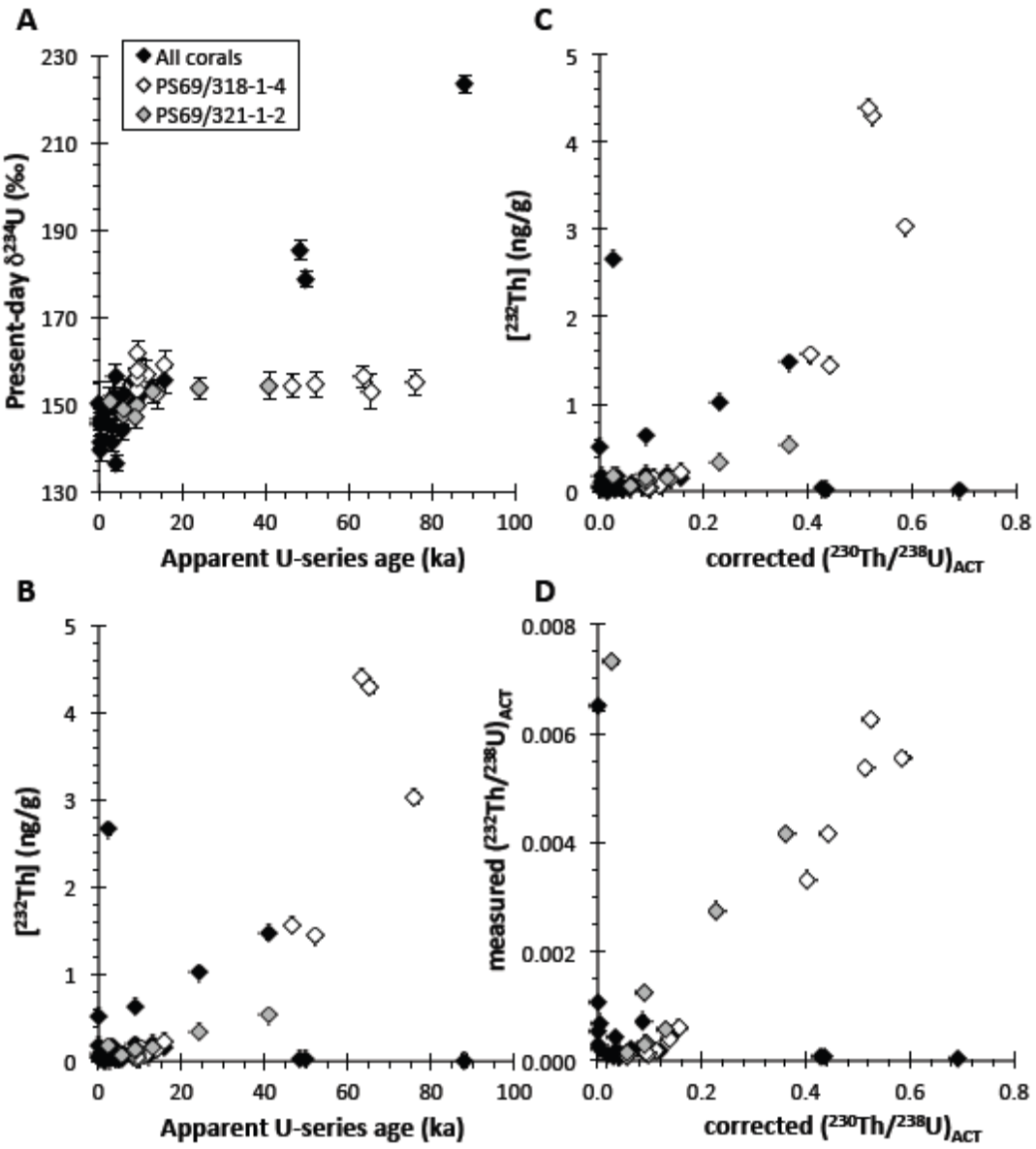

Figure 7.
Gutjahr et al.
Chemical Geology

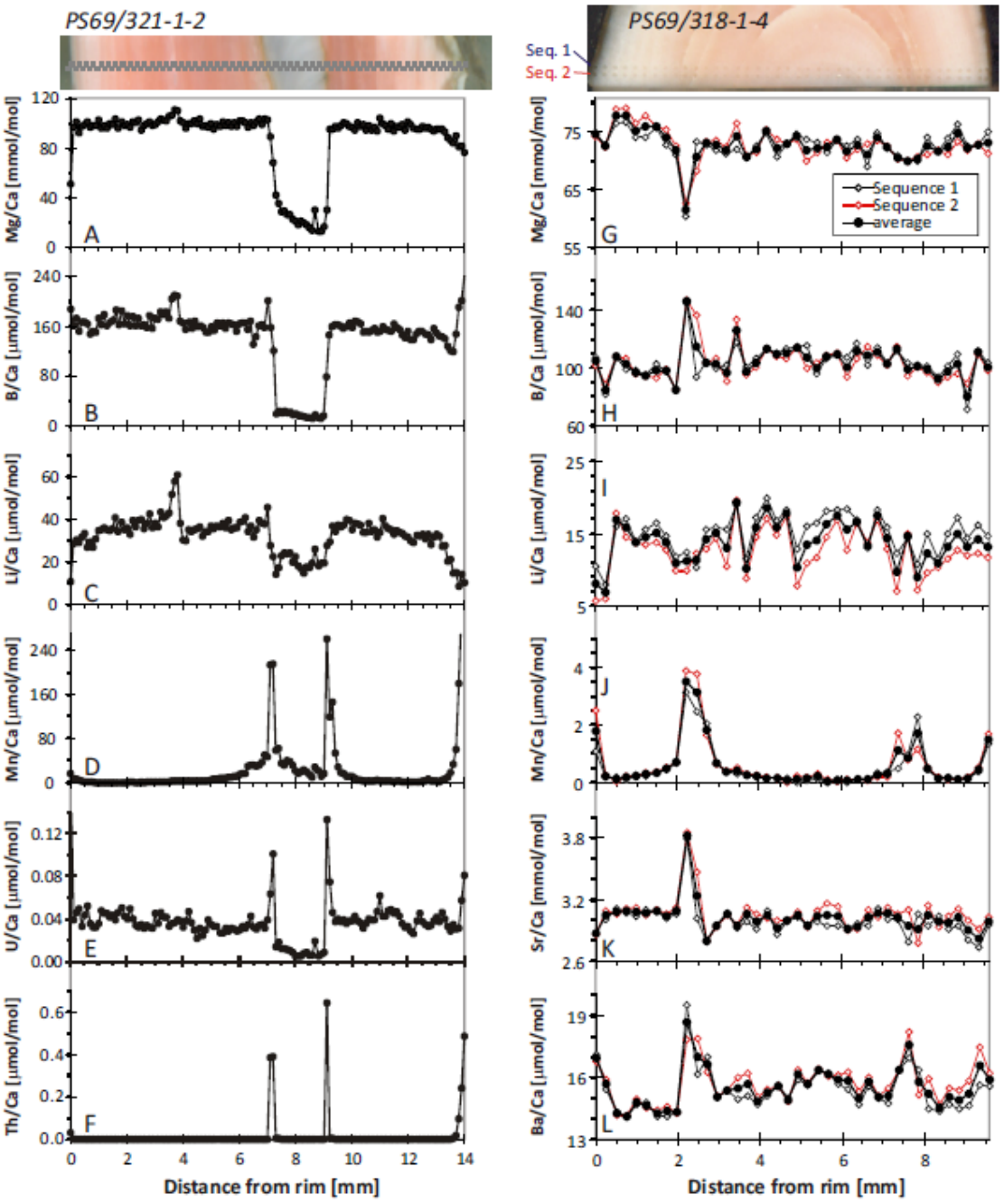

Figure 8.
Gutjahr et al.
Chemical Geology

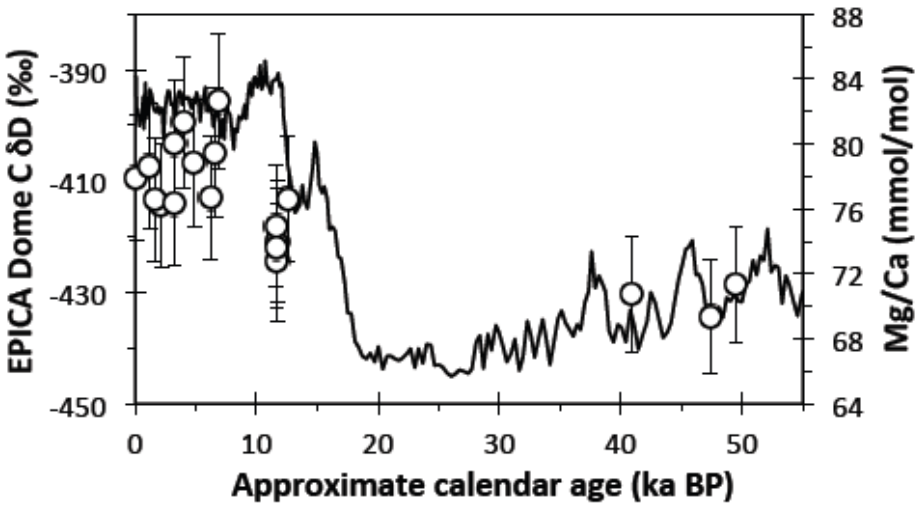

Figure 9.
Gutjahr et al.
Chemical Geology

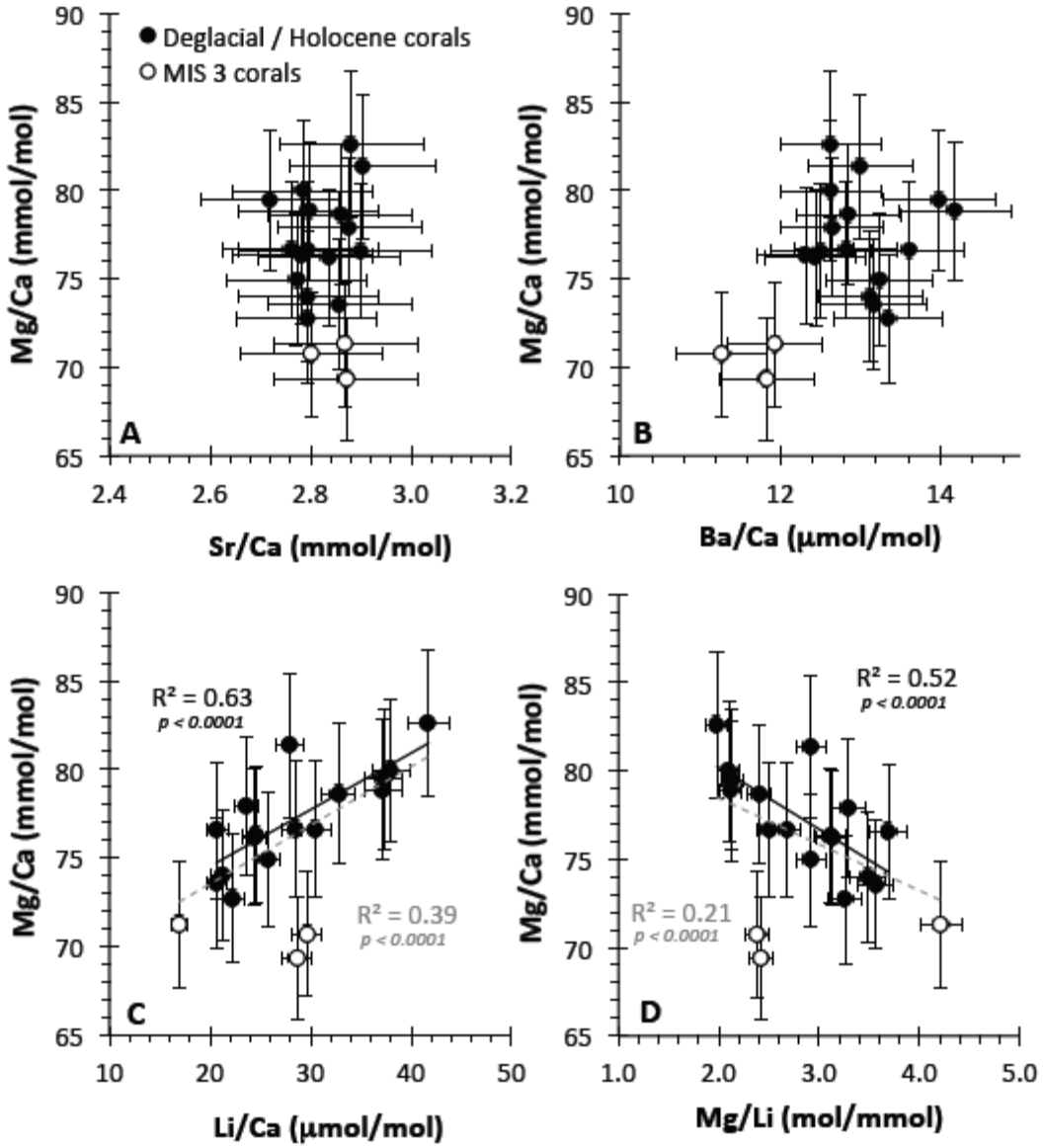

Figure 10.
Gutjahr et al.
Chemical Geology

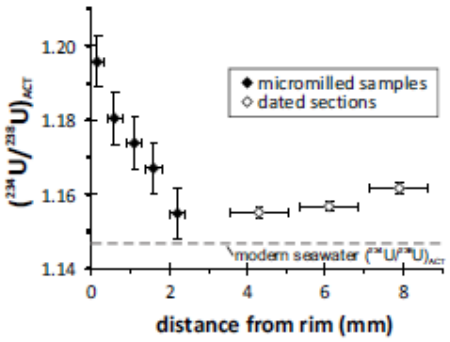

Figure 11.
Gutjahr et al.
Chemical Geology

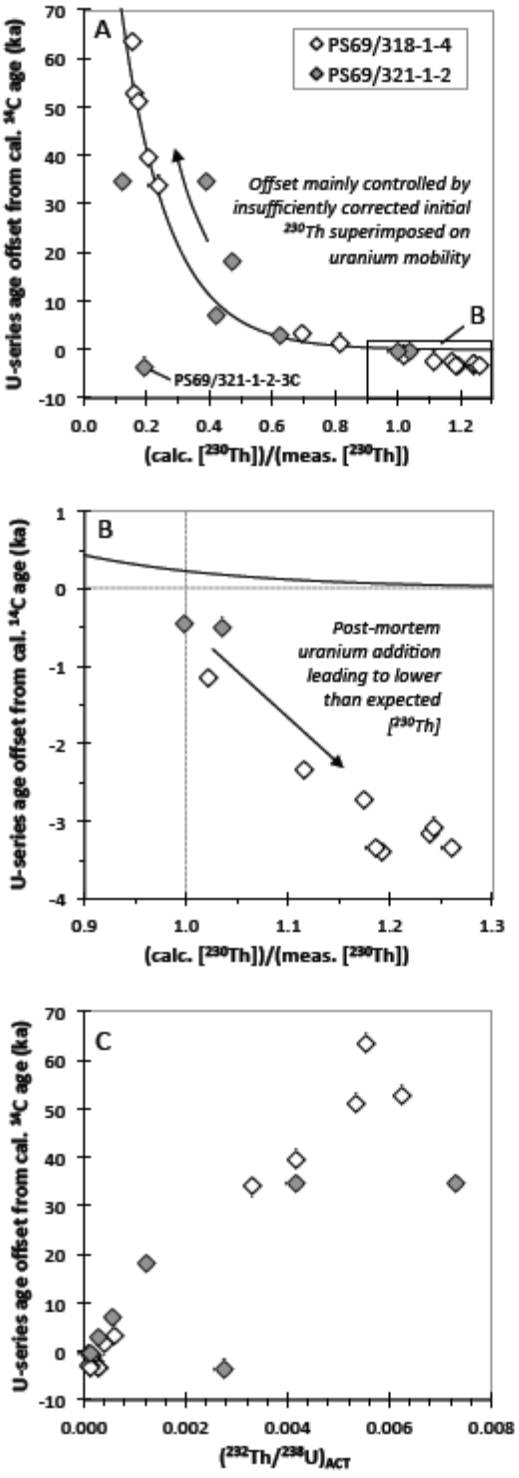

Figure 12.
Gutjahr et al.
Chemical Geology

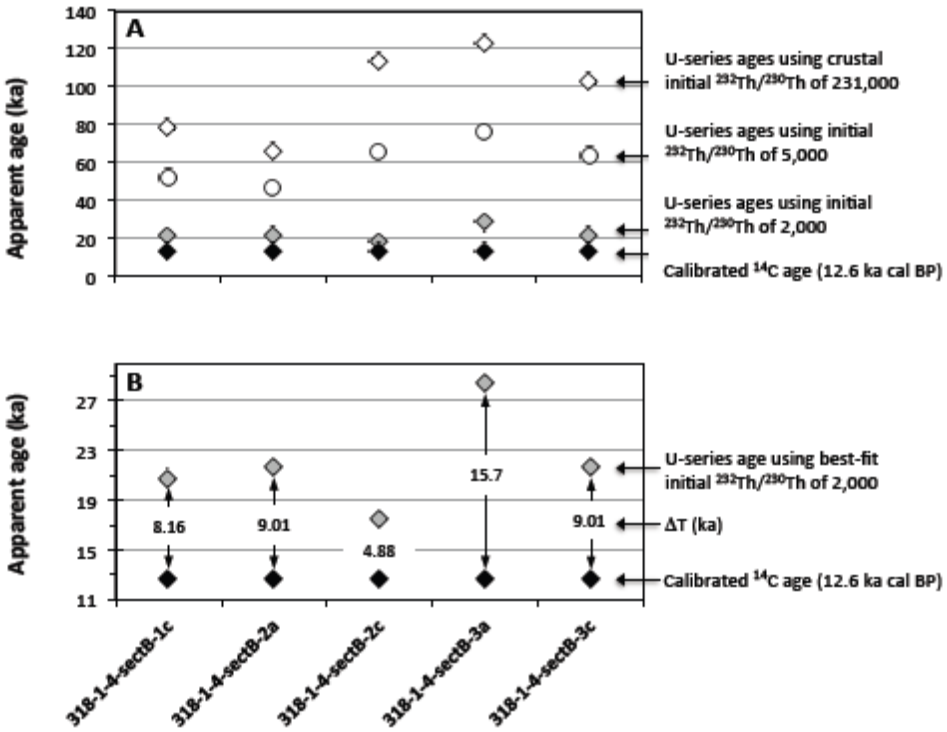

Figure 13.
Gutjahr et al.
Chemical Geology

Table 1. Coral dredging station summary

Cruise / station	Station name	Latitude	Longitude	Max depth m	Min depth m
ANT-XXIII / 4					
PS69/312-1	Seamount 6: E	69°47.47' S	125°56.87' W	1993	1593
PS69/318-1	Haxby Seamount: S	69°08.64' S	123°13.35' W	1788	1480
PS69/319-1	Haxby Seamount: E	69°10.43' S	122°52.60' W	2009	1475
PS69/320-1	Miller Seamount: NW	69°21.09' S	121°52.12' W	2500	2432
PS69/321-1	Miller Seamount: S	69°21.53' S	121°31.94' W	1670	1431
PS69/325-1	Miller Seamount: S	69°27.23' S	120°55.38' W	1560	1527
ANT-XXVI / 3					
PS75/247-2	Haxby Seamount: S	69° 8.14' S	123° 12.73' W	1734	1504
PS75/250-1	Haxby Seamount: S	69° 8.86' S	123° 13.44' W	2014	1499
PS75/251-1	Haxby Seamount: S	69° 10.58' S	122° 51.95' W	2235	1935

Table 2. Compilation of all radiocarbon ages measured on Amundsen Sea cold-water corals

Lab number	Sample number	Radiocarbon age yrs 14C	Calibrated age (a cal BP) Assuming modern reservoir age (1391 yrs)	Calibrated age (a cal BP) Assuming glacial reservoir age (2000 yrs)	Calibrated age (a cal BP) Assuming glacial reservoir age (2500 yrs)
Modern cold-water corals					
ETH-41420	PS69/319-1-2-modern-a	1406 ± 29			
ETH-41421	PS69/319-1-2-modern-b	1376 ± 30			
ETH-41422	PS75/247-2-modern-b	1521 ± 30			
ETH-41423	PS75/247-2-modern-a	1497 ± 30			
Fossil cold-water corals					
ETH-37492	PS69/318-1-4-section1-1B	11890 ± 50	12448 ± 78	11271 ± 50	*10612 ± 64*
ETH-37493	PS69/318-1-4-section1-2B_a	12110 ± 60	12654 ± 56	11722 ± 149	*10987 ± 145*
ETH-37494	PS69/318-1-4-section1-2B_b	12230 ± 55	12745 ± 53	11969 ± 101	*11172 ± 56*
ETH-37495	PS69/318-1-4-section1-3B	12050 ± 55	12607 ± 55	11573 ± 150	*10866 ± 140*
ETH-37496	PS69/318-1-4-section1-4B	11965 ± 50	12533 ± 59	11371 ± 105	*10710 ± 87*
ETH-37497	PS69/318-1-4-section2-1B	11935 ± 55	12501 ± 70	11326 ± 90	*10670 ± 82*
ETH-37498	PS69/318-1-4-section2-2B_a	12160 ± 55	12692 ± 53	11835 ± 123	*11084 ± 115*
ETH-37499	PS69/318-1-4-section2-2B_b	12015 ± 50	12578 ± 54	11482 ± 136	*10796 ± 122*
ETH-37500	PS69/318-1-4-section2-3B_a	12170 ± 55	12699 ± 54	11856 ± 121	*11101 ± 108*
ETH-37501	PS69/318-1-4-section2-3B_b	12025 ± 50	12587 ± 52	11508 ± 139	*10815 ± 127*
ETH-37502	PS69/321-1-	6850 ± 40	6266 ± 31	*5591 ± 32*	*4894 ± 53*

	2-1B				
ETH-37503	PS69/321-1-2-2B	6925 ± 40	6314 ± 34	*5644 ± 37*	*5019 ± 98*
ETH-37504	PS69/321-1-2-3B	6840 ± 45	6257 ± 38	*5584 ± 39*	*4886 ± 53*
ETH-37505	PS69/321-1-2-4B	6820 ± 45	6241 ± 44	*5568 ± 46*	*4869 ± 41*
ETH-37506	PS69/321-1-2-I2B	14210 ± 65	14936 ± 113	13998 ± 88	13572 ± 74
ETH-41442	PS69/318-1-2	11495 ± 40	11713 ± 104	10753 ± 93	*10188 ± 38*
ETH-41443	PS69/318-1-3	6755 ± 35	6172 ± 53	*5506 ± 63*	*4833 ± 23*
ETH-41444	PS69/318-1-5	48785 ± 1230	n/a	n/a	n/a
ETH-41445	PS69/320-1-inner part	37590 ± 340	*41437 ± 345*	40892 ± 351	40431 ± 365
ETH-41446	PS69/320-1-outer part	39800 ± 405	*43343 ± 392*	42822 ± 389	42393 ± 391
ETH-41447	PS69/318-1-N1	11460 ± 40	11625 ± 116	10700 ± 63	*10155 ± 66*
ETH-41448	PS69/318-1-N2	11490 ± 40	11701 ± 106	10745 ± 88	*10184 ± 42*
ETH-41449	PS69/318-1-N3	11475 ± 40	11664 ± 111	10721 ± 74	*10171 ± 53*
ETH-41450	PS69/318-1-N4	4455 ± 35	3290 ± 49	*2525 ± 108*	*1897 ± 36*
ETH-41451	PS69/325-1-#1	45065 ± 510	*47903 ± 479*	47389 ± 482	46963 ± 483
ETH-41452	PS69/325-1-#2	46515 ± 610	*48947 ± 1366*	48578 ± 539	48184 ± 545
ETH-41453	PS69/325-1-#3	47010 ± 665	n/a	48855 0 1591	48565 0 655
ETH-41454	PS75/247-2-#1	5035 ± 35	3959 ± 52	*3250 ± 55*	*2678 ± 71*
ETH-41455	PS75/247-2-#2	7170 ± 35	6580 ± 54	*5920 ± 27*	*5395 ± 57*
ETH-41456	PS75/247-2-#3	5795 ± 35	4974 ± 77	*4170 ± 55*	*3514 ± 49*
ETH-41457	PS75/250-1-#1	11160 ± 40	11201 ± 22	10283 ± 52	*9588 ± 44*
ETH-41458	PS75/251-1-#1	3255 ± 35	1805 ± 45	*1196 ± 51*	*683 ± 18*
ETH-41459	PS75/251-1-#2	3455 ± 35	2018 ± 49	*1339 ± 28*	*881 ± 49*
ETH-41460	PS75/251-1-#3	38495 ± 270	*42225 ± 295*	41697 ± 290	41257 ± 293
ETH-41461	PS75/251-1-#5	7575 ± 35	7088 ± 65	*6349 ± 39*	*5828 ± 60*

n/a = outside calculation range of marine Fairbanks 0107 radiocarbon calibration

Table 3. U-series disequilibrium ages measured on Amundsen Sea cold-water corals

Sample number	^{238}U (ng/g)	±	$\delta^{234}U_{meas}$ (a) (‰)	$\delta^{234}U_{corr}$ (‰)	±	^{232}Th (b) (ng/g)	±	$(^{230}Th/^{238}U)_{meas}$ activity ratio	±		$(^{230}Th/^{238}U)_{corr}$ activity ratio	±	$(^{234}U/^{238}U)_{corr}$ activity ratio	±	apparent age (ka)	±	$(^{234}U/^{238}U)_{initial}$ activity ratio	±	Calibrated ^{14}C age (ka cal BP)	$\Delta T^{(c)}$ (ka)
Modern cold-water corals																				
PS69/319-1-modern1	53.5	0.35	146.4	146.5	2.43	0.17	0.0018	0.0035	0.0002	(1)	0.0026	0.0002	1.147	0.0024	0.25	0.018	1.147	0.0024	n/a	0.25
PS69/319-1-modern2	55.3	0.35	145.5	145.5	2.49	0.05	0.0006	0.0030	0.0005	(1)	0.0028	0.0005	1.146	0.0025	0.27	0.050	1.146	0.0025	n/a	0.27
PS75/247-2-modern1	27.0	0.20	145.9	146.0	3.21	0.04	0.0006	0.0028	0.0012	(1)	0.0024	0.0012	1.146	0.0032	0.23	0.120	1.146	0.0032	n/a	0.23
PS75/247-2-modern2	25.6	2.81	149.4	150.2	4.90	0.51	0.0577	0.0062	0.0028	(1)	0.0010	0.0028	1.150	0.0049	0.10	0.270	1.150	0.0049	n/a	0.10
Fossil cold-water corals																				
PS69/312-1-1-1b	89.8	0.52	156.5	156.6	2.84	0.04	0.0005	0.0476	0.0009	(2)	0.0419	0.0009	1.157	0.0028	4.02	0.089	1.158	0.0029	-	n/a
PS69/312-1-1-1d	92.3	0.48	150.6	150.6	2.65	0.02	0.0003	0.0465	0.0007	(2)	0.0439	0.0007	1.151	0.0027	4.25	0.067	1.152	0.0027	-	n/a
PS69/312-1-2-1b	85.2	0.42	150.7	150.8	2.89	0.19	0.0015	0.1155	0.0012	(2)	0.0885	0.0012	1.151	0.0029	8.72	0.130	1.155	0.0029	-	n/a
PS69/312-1-2-1d	86.6	0.51	155.4	155.5	2.79	0.15	0.0014	0.1772	0.0021	(2)	0.1554	0.0021	1.155	0.0028	15.72	0.240	1.163	0.0029	-	n/a
PS69/318-1-1a	39.2	0.15	141.2	141.2	2.11	0.02	0.0002	0.0128	0.0003	(2)	0.0052	0.0003	1.141	0.0021	0.50	0.030	1.141	0.0021	-	n/a

PS69/318-1-1b	43.3	0.22	139.5	139.6	2.44	0.09	0.0008	0.0168	0.0003	(3)	0.0039	0.0003	1.140	0.0024	0.38	0.030	1.140	0.0024	-	n/a
PS69/318-1-2	90.6	0.43	151.8	151.8	2.47	0.05	0.0004	0.1038	0.0007	(2)	0.0971	0.0007	1.152	0.0025	9.60	0.078	1.156	0.0025	11.713	-2.11
PS69/318-1-3	97.0	0.33	148.7	148.7	2.24	0.02	0.0003	0.0472	0.0005	(2)	0.0442	0.0005	1.149	0.0022	4.28	0.053	1.151	0.0023	6.172	-1.89
PS69/318-1-4 pre	99.8	0.48	154.5	154.6	2.51	0.06	0.0004	0.1282	0.0011	(2)	0.1213	0.0011	1.155	0.0025	12.09	0.120	1.160	0.0026	12.604	-0.51
PS69/318-1-5	155	0.97	223.3	223.3	2.00	0.01	0.001	0.6923	0.033	(2)	0.6917	0.0033	1.223	0.0020	88.1	0.680	1.287	0.0024	~50	~38
PS69/318-1-6	41.7	0.23	145.8	145.8	3.27	0.01	0.002	0.0226	0.0006	(2)	0.0189	0.0006	1.146	0.0033	1.82	0.061	1.147	0.0033	-	n/a
PS69/318-1-7	51.6	0.32	148.3	148.3	2.23	0.00	0.001	0.0171	0.0004	(2)	0.0171	0.0004	1.148	0.0022	1.64	0.036	1.149	0.0022	-	n/a
PS69/318-1-8	94.1	0.56	144.9	144.9	1.91	0.02	0.002	0.0337	0.0004	(2)	0.0316	0.0004	1.145	0.0019	3.06	0.036	1.146	0.0019	-	n/a
PS69/318-1-9-1b	90.9	0.53	152.1	152.2	2.87	0.05	0.0006	0.0435	0.0006	(2)	0.0364	0.0006	1.152	0.0029	3.50	0.061	1.154	0.0029	-	n/a
PS69/318-1-9-1d	118	0.64	152.6	152.6	2.97	0.08	0.0007	0.0718	0.0009	(2)	0.0639	0.0009	1.153	0.0030	6.22	0.096	1.155	0.0030	-	n/a

PS69/318-1-10-2b	80.3	0.40	155.6	155.6	2.54	0.05	0.0005	0.0927	0.0012	(2)	0.0857	0.0012	1.156	0.0025	8.40	0.120	1.159	0.0026	-	n/a
PS69/318-1-10-2d	90.7	0.52	155.6	155.6	2.41	0.04	0.0005	0.0996	0.0009	(2)	0.0937	0.0009	1.156	0.0024	9.22	0.096	1.160	0.0025	-	n/a
PS69/320-1-1a	106	0.82	185.4	185.4	2.12	0.02	0.0004	0.4321	0.0018	(2)	0.4294	0.0018	1.185	0.0021	48.48	0.270	1.213	0.0024	49.0	-0.52
PS69/320-1-1b	110	0.59	178.8	178.8	1.78	0.02	0.0003	0.4381	0.0019	(2)	0.4356	0.0019	1.179	0.0018	49.72	0.280	1.206	0.0020	49.0	0.72
PS69/321-1-1a	127	0.83	141.5	141.6	2.45	0.17	0.0015	0.0500	0.0006	(2)	0.0338	0.0006	1.142	0.0024	3.28	0.061	1.143	0.0025	-	n/a
PS69/321-1-1b	118	0.65	136.6	136.6	1.93	0.03	0.0003	0.0468	0.0004	(2)	0.0441	0.0004	1.137	0.0019	4.31	0.040	1.138	0.0020	-	n/a
PS69/321-1-1c	119	0.56	143.9	143.9	1.77	0.05	0.0004	0.0614	0.0005	(2)	0.0564	0.0005	1.144	0.0018	5.52	0.047	1.146	0.0018	-	n/a
High-resolution sampling, fossil coral PS69/318-1-4																				
PS69/318-1-4-sectA-1a	217	0.87	155.1	155.1	2.91	0.14	0.0013	0.1119	0.0011	(2)	0.1038	0.0011	1.155	0.0029	10.26	0.120	1.160	0.0030	12.604	-2.34
PS69/318-1-4-sectA-1d	113	0.92	157.3	157.4	3.28	0.06	0.0009	0.1063	0.0014	(2)	0.1003	0.0014	1.157	0.0033	9.88	0.150	1.162	0.0034	12.604	-2.72
PS69/318-1-4-sectA-2a	118	0.91	156.8	156.8	3.34	0.07	0.0010	0.1222	0.0016	(2)	0.1154	0.0016	1.157	0.0033	11.45	0.170	1.162	0.0034	12.604	-1.15
PS69/318-1-4-sectA-2d	104	0.42	153.2	153.2	2.71	0.10	0.0008	0.1048	0.0013	(2)	0.0933	0.0013	1.153	0.0027	9.20	0.140	1.157	0.0028	12.604	-3.40
PS69/318-1-4-sectA-3a	141	0.63	161.7	161.7	2.70	0.12	0.0012	0.1054	0.0013	(2)	0.0946	0.0013	1.162	0.0027	9.26	0.130	1.166	0.0028	12.604	-3.34

PS69/318-1-4-sectA-3d	96.0	0.44	156.1	156.2	2.66	0.04	0.0005	0.1008	0.0014	(2)	0.0960	0.0014	1.156	0.0027	9.44	0.150	1.160	0.0027	12.604	-3.16
PS69/318-1-4-sectA-4a	96.6	0.62	158.3	158.4	3.06	0.03	0.0005	0.1005	0.0012	(2)	0.0969	0.0012	1.158	0.0031	9.52	0.120	1.163	0.0031	12.604	-3.08
PS69/318-1-4-sectA-4d	88.2	0.68	157.9	158.0	3.61	0.04	0.0007	0.0991	0.0023	(2)	0.0942	0.0023	1.158	0.0036	9.25	0.240	1.162	0.0037	12.604	-3.35
PS69/318-1-4-sectB-1a	110	0.06	152.2	152.3	3.39	0.14	0.0001	0.1532	0.0013	(2)	0.1379	0.0013	1.152	0.0034	13.88	0.140	1.158	0.0035	12.604	1.28
PS69/318-1-4-sectB-1c	112	0.05	154.2	154.7	2.88	1.43	0.0011	0.5996	0.0038	(2)	0.4427	0.0038	1.155	0.0029	52.16	0.590	1.179	0.0033	12.604	39.6
PS69/318-1-4-sectB-2a	154	0.05	154.0	154.4	2.86	1.56	0.0010	0.5290	0.0028	(2)	0.4042	0.0028	1.154	0.0029	46.56	0.420	1.176	0.0032	12.604	34.0
PS69/318-1-4-sectB-2c	225	9.69	152.2	153.0	3.99	4.29	0.1689	0.7610	0.0043	(2)	0.5255	0.0043	1.153	0.0040	65.37	0.800	1.184	0.0046	12.604	53
PS69/318-1-4-sectB-3a	179	8.43	154.4	155.1	2.73	3.03	0.1471	0.7961	0.0043	(2)	0.5872	0.0043	1.155	0.0027	76.03	0.830	1.192	0.0033	12.604	63
PS69/318-1-4-sectB-3c	268	1.14	155.8	156.4	2.34	4.39	0.0405	0.7184	0.0032	(2)	0.5165	0.0032	1.156	0.0023	63.61	0.560	1.187	0.0027	12.604	51.0
PS69/318-1-4-sectC-1a	119	0.09	159.0	159.1	3.33	0.22	0.0002	0.1797	0.0013	(2)	0.1568	0.0013	1.159	0.0033	15.82	0.150	1.166	0.0035	12.604	3.22
High-resolution sampling, fossil coral PS69/321-1-2																				
PS69/321-1-2-1a	115	5.93	152.8	152.9	2.73	0.20	0.0111	0.1525	0.0011	(2)	0.1314	0.0011	1.153	0.0027	13.18	0.12	1.159	0.0028	6.270	6.91
PS69/321-1-2-1c	111	4.59	147.4	147.4	2.84	0.03	0.0018	0.0623	0.0007	(2)	0.0591	0.0007	1.147	0.0028	5.77	0.07	1.150	0.0029	6.270	-0.50
PS69/321-1-2-2a	114	7.26	149.1	149.1	4.07	0.05	0.0049	0.0646	0.0011	(2)	0.0595	0.0011	1.149	0.0041	5.80	0.11	1.152	0.0041	6.270	-0.47

PS69/321-1-2-2c	121	4.39	149.8	149.8	2.76	0.11	0.0049	0.1028	0.0012	(2)	0.0917	0.0012	1.150	0.0028	9.06	0.13	1.154	0.0028	6.270	2.79
PS69/321-1-2-3a	116	10.79	153.8	154.3	3.13	1.5	0.1368	0.5199	0.0033	(2)	0.3631	0.0033	1.154	0.0031	40.87	0.47	1.173	0.0034	6.270	34.6
PS69/321-1-2-3c	119	8.32	150.0	150.9	3.04	2.7	0.1868	0.1654	0.0019	(3)	0.0277	0.0019	1.151	0.0030	2.66	0.19	1.152	0.0031	6.270	-3.6
PS69/321-1-2-4a	121	7.30	153.4	153.7	2.44	1.01	0.0625	0.3335	0.0020	(2)	0.2301	0.0020	1.154	0.0024	24.17	0.24	1.165	0.0026	6.270	17.9
PS69/321-1-2-4c	166	7.00	146.8	146.9	2.43	0.63	0.0284	0.1361	0.0009	(2)	0.0897	0.0009	1.147	0.0024	8.88	0.10	1.151	0.0025	6.270	2.61
PS69/321-1-2-INT2a	43.2	1.77	169.9	220.1	7.96	37.7	1.6495	26.0283	0.1081	(2)	15.3	0.11	1.220	0.0080	outside range	---	---	---	13.998	n/a
PS69/321-1-2-INT2c	91.7	4.35	154.0	224.4	4.23	109.9	5.0783	41.5736	0.1414	(2)	26.8	0.14	1.224	0.0042	outside range	---	---	---	13.998	n/a

Note:

Analytical errors are 2σ of the mean.

[(a)] $\delta^{234}U = ([^{234}U/^{238}U]_{activity} - 1) \times 1000$.

Decay constants are 9.1577×10^{-6} yr^{-1} for ^{230}Th, 2.826×10^{-6} yr^{-1} for ^{234}U, and 1.55125×10^{-10} yr^{-1} for ^{238}U.

[(b)] The degree of initial ^{230}Th contamination is indicated by the measured $[^{230}Th/^{232}Th]$ activity ratio

U-series ages were calculated using isoplot version 3.0

[(c)] ΔT = (U-series age) - (calibrated ^{14}C age)

[(1)] Non-in situ produced thorium correction for modern corals carried out using only an initial $^{232}Th/^{230}Th$ with crustal compositions.

[(2)] Non-in situ produced thorium correction carried out using an inherited $^{232}Th/^{230}Th$ of 5000 (atomic).

[(3)] Non-in situ produced thorium correction carried out using an inherited $^{232}Th/^{230}Th$ of 10000 (atomic).

Table 4. Various M/Ca and Mg/Li for individual corals measured by solution ICP-MS

Sample #	Li/Ca (mmol/mol)	Mg/Ca (mmol/mol)	Mg/Li (mol/mmol)	Sr/Ca (mmol/mol)	Ba/Ca (mmol/mol)
PS247-2-modern(*)	23.7	77.9	3.29	2.88	12.7
PS69/318 1-2	21.2	74.0	3.49	2.79	13.1
PS69/318 1-3	28.6	76.6	2.68	2.76	12.8
PS69/318 1-4	30.6	76.6	2.51	2.80	13.6
PS69/318 1-5	16.9	71.3	4.22	2.87	11.9
PS69/318 1-6	24.4	76.2	3.13	2.84	12.4
PS69/318 1-7	20.7	76.6	3.69	2.90	12.5
PS69/318 1-8	24.5	76.3	3.11	2.78	12.3
PS69/318--1-N1	25.7	74.9	2.92	2.77	13.2
PS69/318--1-N2	22.3	72.7	3.26	2.79	13.4
PS69/318--1-N3	20.6	73.6	3.57	2.86	13.2
PS69/318--1-N4	38.0	80.0	2.10	2.78	12.6
PS69/325-1-#1	28.6	69.3	2.42	2.87	11.8
PS69/320-1	29.6	70.7	2.39	2.80	11.3
PS69/321-1	37.2	78.8	2.12	2.80	14.2
PS69/318-1	32.8	78.6	2.40	2.86	12.9
PS69/321-1-2	41.7	82.6	1.98	2.88	12.6
PS75/247-2-#1	27.9	81.3	2.92	2.91	13.0
PS75/247-2-#2	37.3	79.5	2.13	2.72	14.0

Only clean inner parts of individual coral specimens have been used for solution-based trace elemental analyses.
(*) Average of eight sub-samples

Table 5. Selected average SRM NIST612 elemental ratios as determined during one session in June 2009

Elemental ratio	Average (n=20)	2 s.d.	2 s.d. (in %)	Difference from reference (in %)
Li/Ca (mmol/mol)	2.93	0.20	6.7%	7.7%
B/Ca (mmol/mol)	1.71	0.13	7.8%	14.8%
Mg/Ca (mmol/mol)	1.33	0.12	8.8%	1.34%
P/Ca (mmol/mol)	640	70	10.9%	-9.4%
Mn/Ca (mmol/mol)	349	10.5	3.0%	5.4%
Sr/Ca (mmol/mol)	0.44	0.02	4.1%	3.91%
Sr/Ba (mol/mol)	3.14	0.13	4.2%	0.50%
Y/Ca (mmol/mol)	211	6.66	3.2%	4.31%
Ba/Ca (mmol/mol)	139	5.82	4.2%	3.41%
Nd/Ca (mmol/mol)	129	4.49	3.5%	-35%
U/Ca (mmol/mol)	78	7.28	9.3%	6.2%
Th/Ca (mmol/mol)	81	2.94	3.6%	6.5%

Diff. To reference refers to the deviation the average elemental ratios compared with GeoRem preferred compositions (Jochum et al. 2011)
Isotopes measured: 7Li, 11B, 26Mg, 31P, 43Ca, 55Mn, 88Sr, 89Y, 138Ba, 146Nd, 232Th, 238U

Structural limitations in deriving accurate U-series ages from calcitic cold-water corals contrasts with robust coral radiocarbon and Mg/Ca systematics

By Marcus Gutjahr, Derek Vance, Dirk L. Hoffmann, Claus-Dieter Hillenbrand,

Gavin L. Foster, James W.B. Rae and Gerhard Kuhn

Highlights (max. 5 points, each bullet point not exceeding 85 characters including spaces)

- Coral radiocarbon contents match local deep water concentrations, ages reliable
- Corals older than a few thousand years affected by U-series open-system behaviour
- Uranium diffusion within and into coral offsetting apparent U-series ages
- Highly variable initial $^{232}Th/^{230}Th$ observed in these Amundsen Sea corals
- Internally homogenous and elevated Mg/Ca potentially controlled by temperature